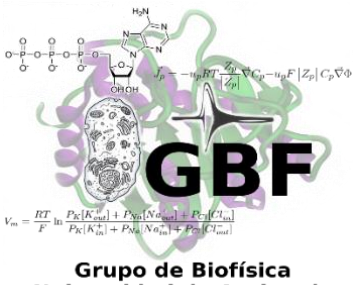

University of Antioquia

Faculty of Exact and Natural Sciences - Institute of Physics

Medellin, Colombia

2021

A research work submitted to obtain the degree of

Master in Physics

Biophysics

by

Jessica Rojas Palomino

Biophysical characterization of the role of synthesized toxins from *Pamphobeteus verdolaga* spider on voltage-gated Ca^{2+} and K^{+} channels by the electrophysiological patch-clamp technique

Supervisor

Prof. Marco A. Giraldo. PhD

Biophysics Group

Co-supervisor

Prof. Juan Camilo Calderón. PhD

PHYSIS Group

Table of contents

Acknowledgements **4**

Abstract **5**

Outline **6**

1. Introduction **7**

2. Project objectives **11**

3. Electrical properties of cell membranes **12**
3.1. The cell membrane 12
How do ions move in and out of cells? 13
What kind of channels are involved in establishing membrane potential? 16

4. Techniques for studying ion channels **19**
4.1. Which techniques would be used to study the ion channel activity? 19
4.2. Basic principle of the patch-clamp technique 21

5. Cardiac cells **26**
5.1. Introduction *26*
5.2. A highly reproducible method for isolating viable cardiomyocytes murine cells from the adult mouse heart 28

6. Calcium currents in cardiac myocytes **31**
6.1. Introduction 31
6.2. Implementation of patch-clamp technique to the study of calcium currents 33

7. Potassium currents in cardiac myocytes **39**
7.1. Introduction 39
7.2. Characterization of voltage-gated potassium channels by the patch-clamp technique 41

8. The role of peptides extracted from venom gland of the spider *Pamphobeteus verdolaga* on voltage-gated calcium and potassium channels **43**
8.1. Introduction 43
8.2. Modulatory features of six novel tarantula peptides isolated from the venom gland of the spider P. verdolaga on Ca^{2+} and K^{+} channels 48

9. Results **50**
9.1. Our Langendorff apparatus makes successful isolation of cardiomyocytes from the adult mouse heart 50
9.2. Isolated cardiomyocytes display normal cardiac currents 51
9.3. The role of peptides of the spider Pamphobeteus verdolaga on voltage-gated Ca^{2+}

and K^+ channels 52

10. Discussion.....57
10.1. Cardiac cells 57
10.2. Ca^{2+} and K^+ currents in cardiac cells 58
10.3. Characterization of the effect of six synthetic peptides on Ca^{2+} and K^+ currents 58

11. Conclusion.....61

12. References.....65

Acknowledgements

The work presented in this research is one of my proudest achievements and would have been impossible if not for all of the individuals that have shown to me support and encouragement along the way. First and foremost, I would like to thank my supervisor, for his guidance, scientific (and life) advices. Prof. Marco A. Giraldo, you have inspired me in ways you will never know. I am immensely grateful for his guidance and contributions of time and ideas to make my Master experience productive and stimulating. I would also like to thank my co-supervisor, Prof. Juan Camilo Calderón. They have been wonderful sources of insight into my research project. I am grateful for the time that they have invested to contribute to my study. The passion and enthusiasm they demonstrate for their research, motivated me to elevate my research and has ultimately served to make me a more well-rounded scientist and researcher.

Alejandro Gomez provided a collaborative, intellectually stimulating and fun environment to learn in as I navigated my way through this experience. His friendship has truly enriched my journey. This Master would have been insurmountable if it were not for the support of him, extraordinaire, multi-talented and ever-knowledgeable. Thus, “Lejito”, your friendship has been invaluable, thank you for being with me in difficult times, thank you for your patience, for guiding me, making me laugh, cry and celebrate together.

Thank you to my amazing family. Mom, you are one of the most inspiring people I have ever known. I am here because of you. ***Dad***, I can’t begin to express how much I miss you. You taught me many things. You taught me to pursue my dreams and to never give up. This research work is dedicated to your memory. Death took you from me to soon (08-02-2021), and I hope that my humble contribution to the field of science research would have made you proud.

I also would like to thank my fellow lab mates and friends, Andres, Jorge and Leo.

“Last but not least, I wanna thank me, I wanna thank me for believing in me, I wanna thank me for doing all this hard work, I wanna thank me for having no days off.

I wanna thank me for always being a giver, And trying to give more than I receive, I wanna thank me for trying to do more right than wrong, I wanna thank me for just being me at all times” Dogg, S.

Abstract

- Six peptide toxins, *vrdg66, vrdg69, vrdg164, vrdg172, vrdg177* and *vrdg183,* have been isolated and purified from the venom gland of the spider *Pamphobeteus verdolaga.* Five of them have disulfide bridged peptides (DBP) and *vrdg66* does not (NDBP). However, *vrdg66* has the higher percentage of bacterial growth inhibition. Combining different techniques, we have investigated the electrophysiological properties of these toxins.

- We examined the effect of *vrdg66, vrdg69, vrdg164, vrdg172, vrdg177* and *vrdg183,* on cardiomyocytes murine cells. These toxins modify the amplitude and gating of ion currents, giving a hypothesis that some peptides could be pore blockers (PBs) (that bind to the extracellular side of the channel pore modifying the amplitude) and others could be gating modifiers (GMs), binding to the voltage-sensing domains (VSD).

- The effects on Ca^+ and K^+ currents in cardiomyocytes were studied using the patch-clamp technique in whole-cell recording configuration, voltage-clamp mode. *vrdg183* decrease the current density with $EC_{50} \sim 0{,}76$ μM (66.67% reduction in maximum amplitude at Ca_V with 1 μM). *vrdg164* (10μM) slow the inactivation process of Ca^+ currents, shift the steady-state activation and inactivation parameters to more positive potentials. vr*dg172* (1 μM) mainly inhibited peak current at K_v over Ca_v channels. *vrdg66, vrdg69 and vrdg177* (1 μM) modulate both K_V and Ca_V. *vrdg6* had the smallest current inhibition percentage, which shows that in NDBP, the modulation of ion channels is poor.
- The amino acid sequences of *vrdg172, vrdg177, vrdg183* are almost identical except for one or two amino acids (data not shown). In all experiments, *vrdg183* was more potent than others suggesting that its conservative residues are important for the toxicity of this *Pamphobeteus verdolaga* toxin.

- The development of novel venom-peptide-based therapeutics or biomolecule requires an understanding of their effects on voltage-gated ion channels. We conclude that *vrdg183* and *vrdg164* are cardiotoxic and combine the classical effects of spider toxins (slowing of inactivation kinetics, shift of steady-state activation and inactivation parameters) with a striking decrease on the ionic selectivity of Na^+ channels.

Outline

Chapter 2 explains how the structure of the cell membrane can be adapted to a classical electrical circuit. Due to the work of Hodgkin and Huxley, it became widely accepted that ions pass across the membrane through channels. This pioneering work was remarkable because gave rise to modern electrophysiology.

In Chapter 3, some methods used during the research are described. Necessary for measuring the membrane voltage or current by accessing the inner cell, is the ability to do intracellular recordings. A procedure to record single channel currents flowing across the membrane is therefore detailed. The equipment, configurations and modes used for patch-clamp stimulations are also described here.

Chapter 4 demonstrate our highly reproducible protocol for isolating viable cardiomyocytes murine cells from the adult mouse heart. The preparation of the cells for patch-clamp experiments is explained. The results Chapter 4 shows viable and functional cardiomyocytes isolated with the characteristic roughly rod-shaped morphology, with rectangular ends and clear cross-striations, as has been reported in the literature.

The results chapter 5 and 6 demonstrate the powerful application of the patch-clamp technique to characterize ionic currents. Calcium and potassium currents are systematically described here. All major biophysical and pharmacological properties of these ionic currents were identical to previously descriptions, confirming the amenability of our isolated cells to patch-clamp studies.

In Chapter 6, we investigated the effects of six peptides isolated from the venom of the spider *Pamphobeteus verdolaga* (we named them: *vrdg66, vrdg69, vrdg164, vrdg172, vrdg177, vrdg183*) on Cav and Kv currents in cardiomyocytes implementing the patch-clamp technique. Our results suggest that some peptides reduced both the amplitude of calcium and potassium currents, other have exquisite selectivity for calcium channels (*vrdg183*) over Kv currents and *vrdg164* caused a shift in the voltage-dependence of activation of calcium channels, which may be an important advance in the development of new therapeutic agents because of the high affinity on cardiac channels.

Chapter 1

Introduction

Electricity plays a role of paramount importance for all excitable cells, from bacteria to man. Excitable eukaryotic cells (e.g., neurons, muscle, and some neuroendocrine cells) have rather specialized roles in intracellular metabolism, secretion of hormones, signal transduction, the sensation of the environment, gene expression, muscle contraction, and protein degradation, by generating electrical signals in terms of changes in the membrane potential. Since the studies of Galvani in the late 1700s, the idea of electricity having an important role (or effect) in living organisms has defined the scientific lives of many researchers (Hodgkin et al., 1952; Moore en Cole, 1963; Tasaki en Singer, 1968). They constructed the knowledge that permits us to have the very dynamic area that we have today. Electrical signals are generated by ions that diffuse across the membrane through channels to initiate and propagate the voltage spikes known as action potentials (AP). Cellular Ca^{2+} movement, for example, is especially involved in mediating or modulating the process of excitation-contraction coupling (ECC) in muscle cells. In addition, sodium and K^+ channels are essential for initiating and restoring the AP, respectively, and they are involved in multiple physiological processes (Catterall, 1995). Since the first voltage-gated sodium channel was cloned from the electric eel *Electrophorus electricus* in the early 1980s (Noda et al., 1986), the application of several biochemical, biophysical, and molecular genetic methods have allowed understanding the protein structure of voltage-gated ions channels (VGIC) and their molecular mechanisms related with voltage-dependent activation, inactivation, selective ion conductance, and long-term modulation.

The pore-forming subunits of VGIC are integral membrane proteins that allow the flux of inorganic ions (e.g. Na^+, K^+, Ca^{2+} and Cl^-) down their electrochemical gradient through the cell membrane. Ion channels share a common structure: organized into domains, they are typically formed by six α-helical transmembrane segments (S1-S6), in which the ion conduction pathway is located between the segments five and six. Repeated motifs of positively charged amino acid residues form the S4 segment that moves in response to changes in the membrane electric field to initiate a conformational movement that opens the pore region (Catterall, 1995; Yu et al., 2005). Auxiliary β, γ, δ and ε subunits associate with the α-subunit to modify the channel properties, which include the kinetics and voltage dependence gating, membrane surface expression, pharmacology, and selectivity.

Eleven genes (SCN1A–SCN11A) encode a family of nine mammalians functionally expressed voltage-gated sodium channels (VGSC; $Na_v1.1$–$Na_v1.9$), which have been identified by complementary techniques, such as electrophysiological recording, biochemical purification, and cloning (Catterall, 1995; Goldin et al., 2000). For voltage-gated K^+ channels (VGPC), 40 different isoforms are known, classified into 12 distinct subfamilies based on their amino acid sequence homology, Shaker ($K_v1.1$-1.8), Shab ($K_v2.1$-2.2), Shal ($K_v3.1$-3.4), Shaw ($K_v4.1$-$K_v4.3$), KCNQ ($K_v7.1$-7.5) and hERG ($K_v10.1$-10.2, $K_v11.1$-11.3, $K_v12.1$-12.3) (Choe, 2002; Coetzee et al., 1999; Gutman et al., 2003; Yu et al., 2005). This superfamily of VGIC is essential in many aspects of cellular regulation and play important roles in signal transduction. The family of voltage-gated Ca^{2+} channels (VGCC) initiate many different physiological events. Four α1-subunits have been cloned and classified for the L- type Ca^{2+} channel, namely $Ca_v1.1$, $Ca_v1.2$ $Ca_v1.3$, and $Ca_v1.4$, three Ca_v2 channels have been found ($Ca_v2.1$ or P-/Q-type, $Ca_v2.2$ or N-type, and $Ca_v2.3$ or R-type channels) (Senatore et al., 2016) and three genes encoding for T-type channels have been named $Ca_v3.1$, $Ca_v3.2$, and $Ca_v3.3$ (Mesirca et al., 2015).

Mutations in the genes encoding the VGIC have been associated with a wide variety of diseases, so-termed channelopathies. These functional abnormalities are known to cause dysfunctions of the neurological system (e.g., epilepsy, migraine, pain disorders), the cardiovascular system (e.g., arrhythmias, long QT and short QT syndromes, atrial fibrillation, slow ventricular conduction), the respiratory system (e.g., cystic fibrosis), the endocrine system (e.g., diabetes), the urinary system (e.g., Bartter syndrome, diabetes insipidus, autosomal-dominant polycystic kidney disease, and hypomagnesemia with secondary hypocalcemia), the immune system (e.g., myasthenia gravis, and anti-NMDA [N-methyl-D-aspartate] receptor encephalitis) and VGSC has been associated with aggressive metastatic carcinoma of prostate ($Na_v1.7$) and breast ($Na_v1.5$) (Fraser et al., 2014; Onkal en Djamgoz, 2009). Therefore, the VGIC are clear molecular targets for a broad range of potent biological and therapeutic agents as sites of action for drugs and potential disease markers (McGivern, 2007; Williams et al., 2006; Wulff et al., 2009).

Sodium channels are the molecular targets for several groups of neurotoxins, which alter channel function due to their high affinity and specificity. Nowadays six different neurotoxin binding sites have been identified on VGSC (Catterall et al., 2007). For that reason, toxins also provide powerful tools to study the structure and the function of ionic channels. Moreover, they constitute a valuable source for peptides with potential therapeutic use and applications as algaecides, herbicides, and insecticides (King et al., 2008a).

To date, many toxin peptides acting especially as voltage-gated channels of sodium, K^+, and Ca^{2+} have been identified from animals, such as scorpions, snails, and spiders (Adams, 2004; Frazão et al., 2012; Lewis et al., 2012; Olivera, 1997; Possani et al., 2000). Spider venoms are cysteine rich polypeptides and their properties and structures have been reviewed in earlier studies (Herzig et al., 2011; Huang et al., 2007; Klint et al., 2012; Rash en Hodgson, 2002). Despite their physiological importance and therapeutic relevance, electrical properties (resulting from the interaction between ion channels and molecular targets for a wide range of potent biological spider toxins) have historically been difficult to monitor, due to the limitations of methods.

Ionic currents have been measured since 1952 after the pioneering work of Hodgkin and Huxley (Hodgkin en Huxley, 1952a; Hodgkin et al., 1952) who were awarded the Nobel Prize in 1963. Later, the development of the patch-clamp technique in the late 1970s (Neher en Sakmann, 1976) and its variant, including the whole-cell configuration, has facilitated the manipulation of the cytosolic space, allowing the use of electrical stimuli in different cell types, including cardiac muscle fibers. This method, when operating in the *voltage-clamp* mode, allows the measurement of ionic currents arising either from single channels or through the whole assembly of ion channels expressed in the membrane of excitable cells. In response to potential (voltage) steps, the channels show conductance changes that can be quantitatively described by the Hodgkin and Huxley equations (Hodgkin en Huxley, 1952b). These changes have permitted a detailed mechanistic analysis of the gating (e.g., opening and closing) of multiple types of ion channels (e.g. VGSC, VGCC and VGPC). Hence, the patch-clamp technique has rapidly become the *gold standard* in investigating ion channels (Farre en Fertig, 2012; Farre et al., 2007; Fertig et al., 2002; Lu en An, 2008; Willumsen et al., 2003; Zhang et al., 2015).

Previous patch-clamp studies have shown that peptides derived from spider venoms act either as pore blockers (PBs) (that bind to the extracellular side of the channel pore) or as gating modifiers (GMs) (that bind to the voltage-sensing domains of VGIC channels) to modify the gating associated with channel activation and inactivation. Besides, several studies have investigated the nature of the interaction between lipids, PBs and GMs, including the position of the peptide in the lipid bilayer (Agwa et al., 2020; Männikkö et al., 2018; Zhang et al., 2018). Based on these studies, it has been suggested that many gating modifier peptides are located at the water–lipid interface and that their orientation in the membrane and interactions are important for binding to the voltage sensing domain (VSD). Further evidence suggests that the GMs and PBs do not necessarily insert into the lipid bilayer. Taken together, these studies provide strong evidence that toxins are potent and selective inhibitors of VGIC. However, compared with other animals, few spider toxins with activity against VGIC have been identified, and for most of them, the mechanisms by which spider toxins interact with these channels has not been fully elucidated (Henriques et al., 2016).

In 2016, a detailed taxonomic study allowed to recognize and describe *Pamphobeteus verdolaga* as a new species from the Andean region of Colombia (Estrada-Gomez et al., 2013). Lately, venomic, transcriptomic, and bioactivity analyses of *P. verdolaga* venom was associated with complex disulfide-rich peptides that modulate the activity on voltage-gated Ca^{2+} channels (VGCC; $Ca_v2.2$, $Ca_v3.2$), and VGSC ($Na_v1.7$) (Cifuentes et al., 2016). However, the study of the effects of these peptides on VGIC using patch-clamp technique have never been done. In addition, the interactions of these toxins with the lipid bilayers must be investigated.

The Biophysics (Institute of Physics), PHYSIS (Faculty of Medicine) and Ophidism (Faculty of Chemical and Food Sciences) Groups of the University of Antioquia, joined forces to investigate the ability of peptides from the gland of *P. verdolaga* to inhibit and control the growth of resistant microorganisms and, in this way, propose the development of new biomolecules with therapeutic potential.

In this study, we used whole-cell patch-clamp technique to investigate the effect that six peptides from the venom gland of the Colombian *Pamphobeteus verdolaga* spider, can exert on voltage-gated calcium and potassium channels of murine cardiomyocytes. These cell types were chosen because they express many of the known isoforms ($Na_v1.1$, $Na_v1.3$, $Na_v1.5$, $Na_v1.6$, $Ca_v1.2$ $Ca_v1.3$, $Ca_v3.1$, $Ca_v3.2$, $K_v1.1$, $K_v1.2$, $K_v1.4$, $K_v1.5$, $K_v2.1$, $K_v4.2$ and $K_v4.3$). Our results showed that, some peptides have effects on calcium and potassium currents, and others are highly selective for calcium channels. The effect or selectivity of new toxins for ion channels may provide an important tool for translation into therapeutic agents or being useful tools for studying channel structure and activity. Moreover, the selectivity of new toxins for calcium channels (over potassium) may provide an important tool for the modulation of the cardiac system, especially in cases in which blocking of calcium channels is required.

Chapter 2
Project objectives

The overall objective of this study was to investigate the effects of synthesized peptides, derived from the venom gland of *P. verdolaga*, on VGC and VGP channels of cardiomyocytes murine cells.

The specific objectives of this project were:

1. To isolate mouse cardiomyocytes by using the Langendorff technique of retrograde heart perfusion for patch-clamp experiments.
2. To characterize the effects of *P. verdolaga* spider peptides on Ca^{2+} currents by applying the patch-clamp technique in whole-cell recording configuration, voltage-clamp mode.
3. To evaluate the effects of *P. verdolaga* spider peptides on K^{+} currents by applying the patch-clamp technique in whole-cell recording configuration, voltage-clamp mode.

Chapter 3
Electrical properties of cell membranes

The structural and functional basic units in living beings are cells. These systems have compartments isolated from each other and from the extracellular medium by biological lipidic membranes. There are around 210 distinct human cell types with functions that range from structure and support to reproduction. Nevertheless, their membranes have many similar structures (Fig. 1). There kinetic models that quantitatively explains how the structure of the cell membrane can be adapted to a classical electrical circuit. The basic features of this circuit can be described by the Hodgkin-Huxley (H-H) equations. This pioneering work was remarkable because gave rise to modern electrophysiology.

3.1. The cell membrane

The modern concept of the membrane has its origin from a model proposed by S. Jonathan Singer and Garth Nicolson in 1972 (Singer en Nicolson, 1972), which consists of a negative lipid bilayer with integral or peripheral hydrophobic proteins incorporated. The bilayer defines the cell space and maintains the differences between cytoplasm and its extracellular environment. It also generates and preserves differences in the concentration of a series of ions that are important for cellular activity. Therefore, membranes constitute a highly specific and selective barrier for the entry of nutrients into the cell, and controls the exit of waste products. In addition, most of the membrane proteins contain attached sugar residues that act as receptors for neurotransmitters, ion channels, transporters, adhesion or recognition molecules, etc. The model, known as the *fluid mosaic model* is general for all types of biological membranes (Fig. 1). However, the most recent membrane model, the lipid rafts, demonstrates that the bilayers are specialized assemblies composed of sphingolipids, cholesterol, and fluctuating proteins that can be stabilized to perform cell signaling and specific trafficking of proteins (Lingwood en Simons, 2010).

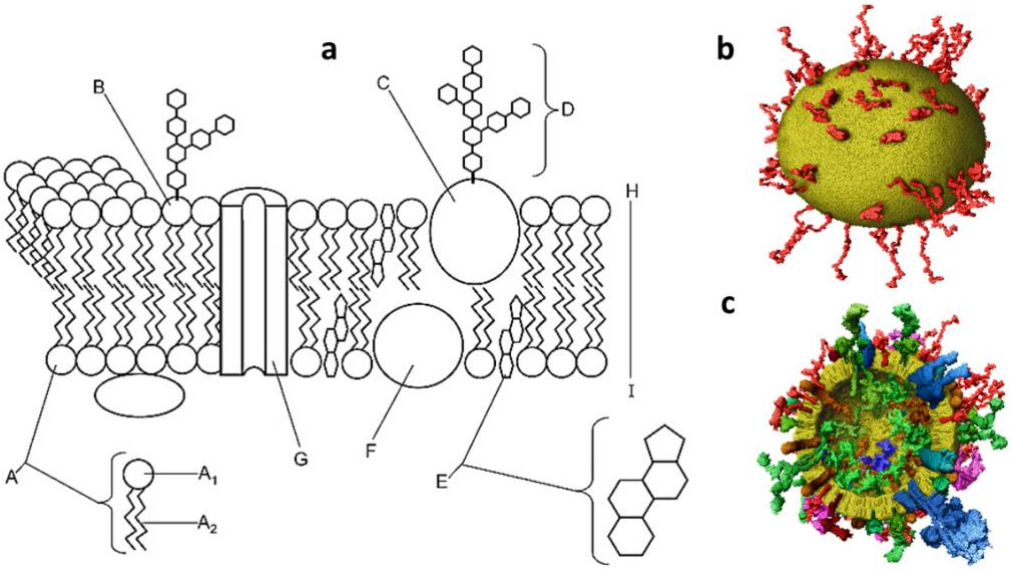

Fig. 1. The fluid mosaic model. **a** A typical eukaryotic cell. (**A**. Phospholipid, **A1**. Phosphate head (hydrophilic), **A2**. Fatty acid tail (hydrophobic), **B**. Glycolipid, **C**. Glycoprotein, **D**. Polysaccharide, **E**. Cholesterol, **F**. Integral protein, **G**. Integral protein channel, **H-I**. Phospholipid bilayer. **Unlabeled**. Peripheral protein); **b** View of the surface density of a vesicle that supports the dynamic portrait of the mosaic model structure. **c** Vesicle sectioned in the middle. Taken from (Takamori et al., 2006).

The phospholipid bilayer can be permeable to small molecules, but is almost fully impermeable to certain ions (e.g. Na^+, K^+, Ca^{2+}, Cl^-) and large molecules, such as glucose. The diffusion of small uncharged molecules occurs in favor of their concentration gradient (i.e. following the least energy principle). The osmotic flow of water emerges from a concentration gradient of non-diffusible molecules across the membrane. In contrast, the flow of large molecules and ions, which do not diffuse through the phospholipid bilayer, is allowed by the presence of transmembrane proteins (Boron en Boulpaep, 2012). This movement of charged particles gives rise to an electric current. Among the great diversity of transmembrane proteins, ion channels and other active transporters, are relevant in the context of this work.

How do ions move in and out of cells?

Signaling of excitable cells relies on the movement of asymmetrically distributed charges that are carried by ions across the cytoplasm and the extracellular space (Hodgkin en Huxley, 1952c). Fig. 2a depicts a schematic representation of the protein channels and their respective ion concentrations across the membrane of mammalian excitable cells. These asymmetric concentrations result in a transmembrane potential (V_m), and their flux occurs by diffusion until the chemical and electrical driving forces are exactly balanced.

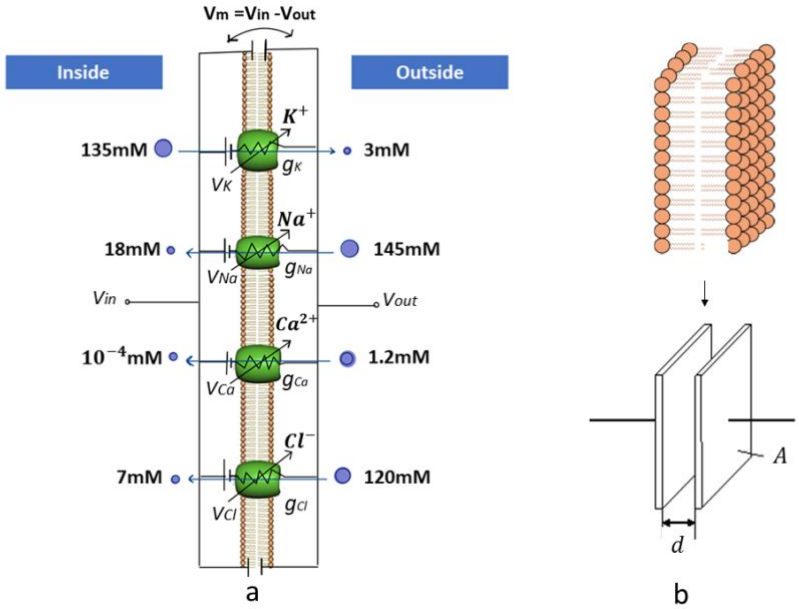

Fig. 2. Electrical properties of model cell membrane (own elaboration). **a** Average values for electrolyte concentrations in extracellular and intracellular fluid. At the same time, schematic representation of Hodgkin and Huxley equivalent circuit of a cell membrane (Hodgkin and Huxley, 1952); **b** Above is a capacitor that is formed by a piece of lipid membrane. Down is an idealized capacitor, which is formed by two parallel plates, each with an area A and separated by a distance d. The capacitance of 1 cm^2 of most cell membranes is ~1 µF.

At the electrochemical equilibrium, the Gibbs free energy is zero by definition, and the chemical and voltage driving forces are exactly balanced. In this equilibrium, the potential is usually called the **Nernst potential** (or **reversal potential**)**,** which is specific for each particular ion (Boron en Boulpaep, 2012).

$$V_{Nernst} \equiv V_{rev} \equiv V_{ion} = \frac{\mathrm{RT}}{\mathrm{zF}} \ln \frac{[ion]_{out}}{[ion]_{in}} \tag{1.1}$$

where *R* and *F* are the gas and Faraday's constants, respectively; *T* is the temperature in Kelvin, and *z* the valence of the considered ion (e.g. *z* equals 1 for Na^+ and K^+, 2 for Ca^{2+} and -1 for Cl^-). Although there are different types of cells, the concentration distribution of the four major ions in most animals follows the same rule: $[K^+]_{in} > [K^+]_{out}$, $[Na^+]_{in} < [Na^+]_{out}$, $[Ca^{2+}]_{in} < [Ca^{2+}]_{out}$, $[Cl^-]_{in} < [Cl^-]_{out}$ (Fig. 2a.) (Johnston en Wu, 1995).

At rest, the **membrane (or resting) potential** (V_m) is defined by the **Goldman-Hodgkin-Katz (GHK**) equation (Eq. 1.2), which takes into account all the ion species (Boron en Boulpaep, 2012; Johnston en Wu, 1995);

$$V_m = V_{rest} = \frac{\mathrm{RT}}{\mathrm{F}} \ln \left(\frac{P_{Na^+}[Na^+]_{out} + P_{K^+}[K^+]_{out} + P_{Cl^-}[Cl^-]_{in}}{P_{Na^+}[Na^+]_{in} + P_{K^+}[K^+]_{in} + P_{Cl^-}[Cl^-]_{out}} \right) \tag{1.2}$$

Any modification of membrane *permeability* to ions (P_{Na^+}, P_{K^+}, P_{Cl^-}), changes the resting potential of the cell; some ions by hyperpolarizing the cell, others depolarizing it. The main ion in setting the resting membrane potential is K^+, thus the V_{rest} value is quite close to the V_{Nernst} of K^+. When the cell is solely permeable to K^+ (i.e. $P_{Na^+} = P_{Cl^-} = 0$ in Eq. 1.2), it becomes hyperpolarized. In the same way, when the cell membrane is mainly permeable to Na^+, the cell is depolarized.

For a cell that is permeable to K^+, Na^+ and Cl^- ions, typical values of resting membrane potentials are between -90 and −70 mV (e.g. squid giant axon permeabilities P_{K^+}: P_{Na^+}: P_{Cl^-} = 1: 0.03: 0.1) (Huxley en Hodgkin, 1952), but it can rise up within milliseconds to +44 mV during an AP (e.g. squid giant axon permeabilities P_{K^+}: P_{Na^+}: P_{Cl^-} = 1: 15: 0.1) (Hodgkin and Huxley, 1952a; Hodgkin and Huxley, 1952b; Hodgkin and Huxley, 1952d; Hodgkin and Huxley, 1952e). The rapid transients in V_m are possible due to the high density of ion channels in the bilayer (typically 10 –1000 per Cm^2) (Daroff, R. B., & Aminoff, 2014).

Due to the low $[Ca^{2+}]$, the permeability of the cell membrane to this ion during rest is also low (<< 0.1% of K^+ permeability), thus Ca^{2+} has no influence in the GHK equation (Eq. 1.2) (Daroff, R. B., & Aminoff, 2014).

The electrical properties of biological membranes can also be characterized by parameters of a classical electric circuit (Fig. 2a) (Hodgkin en Huxley, 1952c). The basic features of this circuit can be quantitatively described by the H-H equations. Their circuit model represents the sodium, K^+, and leakage channels as electric resistances (with a given conductance value of 1/R). The ion flux defines the ionic current I_{ion}. The conductance of the channel (g_{ion}), the membrane potential (V_m) and the ion reversal current (I_{ion}) follow the Ohm's law (Boron en Boulpaep, 2012):

$$I_{\text{ion}} = g_{\text{ion}}(V_{\text{m}} - V_{\text{Nernst}}) \tag{1.3}$$

Under physiological conditions, the amplitude of this current through a single VGIC is in the order of 1 pA (10^{-12} A). This number corresponds to a quite high flux (~10^7 ions/s) (Daroff, R. B., & Aminoff, 2014).

The particular structure and morphology of the membrane make it suitable for electrical modeling. The bilayer is a dielectric material (phospholipids) that separates two conductive media. Charged ions accumulate at both sides (intra and extracellular), acting as an authentic

capacitor that can be approximated to parallel plates (Eq. 1.4, Fig. 2c) (Boron en Boulpaep, 2012; Hodgkin en Huxley, 1952b; Johnston en Wu, 1995).

$$C_m = \frac{\varepsilon\varepsilon_0 A}{d} \tag{1.4}$$

A is the area of one plate in square centimeters, *d* is the distance between the plates in centimeters, ε=2.1 is the natural dielectric constant of lipids, and ε_0=8.85x10-12 F/m is the electrical permittivity of vacuum.

Using Eq. 1.4, the charge distribution across the membrane can be calculated. This reflects the capacitive current I_C (Boron en Boulpaep, 2012),

$$I_{\mathrm{C}} = I_{\mathrm{m}}(t) = \frac{d(V_{\mathrm{m}}C_{\mathrm{m}})}{dt} \tag{1.5}$$

The total current I_{t} may be split in a capacitive current I_C which charges the lipid bilayer and further currents which pass through the ion channels. Considering the case of the four ion channels represented in Fig. 2a and implementing the Eqs. 1.3 and 1.5, and Kirchhoff's current law gives (Boron en Boulpaep, 2012):

$$I_{\mathrm{t}} = I_{\mathrm{C}} + I_{\mathrm{Na}} + I_{\mathrm{K}} + I_{\mathrm{Ca}} + I_{\mathrm{Cl}} = 0 \tag{1.6}$$

Where the total expanded membrane current is therefore expressed as:

$$I_{\mathrm{t}} = \frac{dV_{\mathrm{m}}C_{\mathrm{m}}}{dt} + g_{Na}(V_{\mathrm{m}} - V_{\mathrm{Na}}) + g_K(V_{\mathrm{m}} - V_K) + g_{Ca}(V_{\mathrm{m}} - V_{\mathrm{Ca}}) + g_{Cl}(V_{\mathrm{m}} - V_{Cl}) \tag{1.7}$$

Eq. 1.7 is at the basis of electrophysiological modeling and the study of cell dynamics.

What kind of channels are involved in establishing membrane potential?

One of the most significant outcomes of the work of H-H, was their hypothesis of moving charged particles as the trigger of the carriers' activation (Hodgkin and Huxley, 1952). They proposed that the diffusive property of the membrane occurs at discrete sites, called "carriers". Later, these carries were identified as ion channels. Moreover, they experimentally observed that the implicated channels were of the *voltage-gated channel* family (Huxley, 1952a; Huxley, 1952b; Huxley & Hodgkin, 1952).

Gates in the voltage-gating ion channels are opened or closed by membrane potential changes. If a specific ion can pass through the gate, it is in open position. A number *m* is defined as the probability that an individual gate is in the permissive state (open), thus 1-*m* is the fraction in the

non-permissive state (closed). For Na^+ current activation, three identical activation gates (~m^3) move from closed to open position at depolarized V_m. The change in time of m is described by:

$$\frac{dm}{dt} = \alpha_m(\mathrm{V})(1-m) - \beta_m(V)m \tag{1.8}$$

where α and β are the V_m-dependent opening and closing transition rates.

A decrease in the current, shortly after activation (or inactivation state) is interpreted by using a single gate with open probability h. At hyperpolarized potentials, h is fully open. The inactivation is independent of m and the permeability is:

$$g_{\mathrm{Na}} = \overline{g_{\mathrm{Na}}} m^3 h \tag{1.9}$$

where $\overline{g_{\mathrm{Na}}}$, is the maximum conductance (g_{Na}, Fig. 3c).

For I_K, the driving force depends on the transmembrane K^+ gradient. Additionally, the activation is more sigmoidal-like and inactivation is not observed (g_K, Fig. 3c). For the opening probability of the K^+ activation gate, the variable n is assigned. This behavior requires four identical independent gates, n^4:

$$\frac{dn}{dt} = \alpha_n(\mathrm{V})(1-n) - \beta_n(V)n \tag{1.10}$$

$$g_{\mathrm{k}} = \overline{g_{\mathrm{k}}} n^4 \tag{1.11}$$

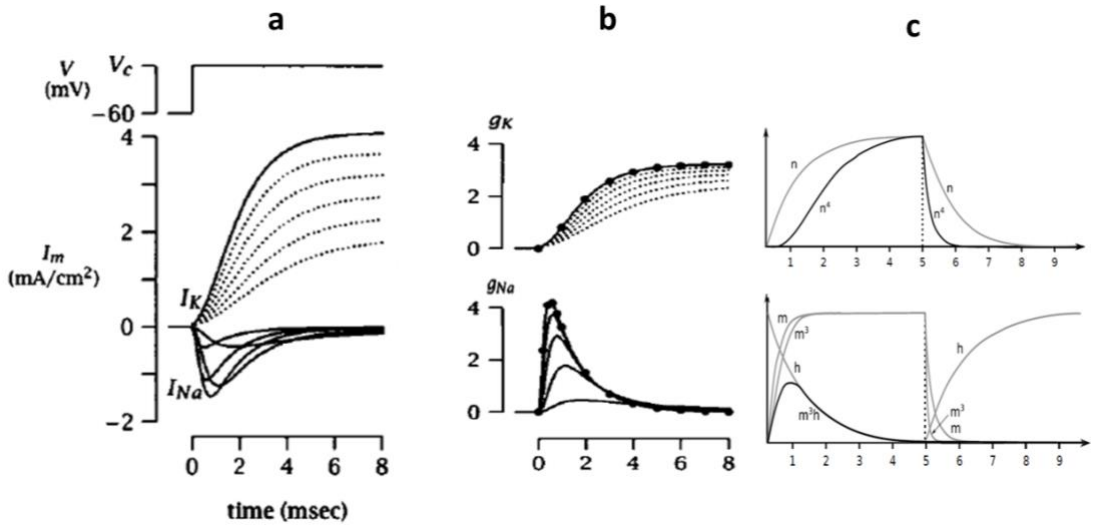

Fig. 3. Voltage and time dependence of ionic conductances; comparison of the Hodgkin–Huxley model with experiments; **a** Changes of sodium and K^+currents associated with different depolarizations; **b** g_{Na} and g_K were plotted by solving the conductance of Eq. 1.3; **c** g_{Na} and g_K were plotted by using the H-H conductances (Hodgkin en Huxley, 1952c; Johnston en Wu, 1995). The x-axis at **b** and **c** is time.

In addition, there is a leakage constant, which does not vary with time or conductance, and is assumed for current not carried by I_{Na} or I_{K}. The leakage current I_{L} is:

$$I_{\mathrm{L}} = g_{\mathrm{L}}(V_{\mathrm{m}} - V_{\mathrm{L}}) \tag{1.12}$$

Then, replacing Eq. 1.9, 1.11 and 1.12 into Eq. 1.6, the total expanded membrane current is therefore expressed as:

$$I_t = C_m \frac{dV_m}{dt} + \overline{g_{Na}} m^3 h(V_m - V_{Na}) + \bar{g}_k n^4 (V_m - V_K) + g_L (V_m - V_L) \qquad (1.13)$$

To summarize, this model is potentially capable of reproducing Eq. 1.7 according to the kinetics of the included voltage-channels. For their discoveries, Hodgkin and Huxley were awarded with the Nobel Prize in Physiology and Medicine in 1963 (The Nobel Prize in Physiology or Medicine, 1963).

Chapter 4
Techniques for studying ion channels

Due to the work of Hodgkin and Huxley, it became widely accepted that ions pass across the membrane through gates. The present chapter contains a brief overview of several experimental techniques available for ion channels electrophysiology. Its main goal is to familiarize the reader with the most relevant methods and systems used during the present investigation.

Which techniques are used to study the ion channel activity?
Nuclear magnetic resonance, X-ray crystallography, neutron diffraction and electron microscopy are experimental methods that allow obtaining a detailed 3-D characterization of protein structures. The best resolution way of forming three-dimensional images of molecules with bonding atomic detail is crystallography.

Determining the structure of biological macromolecules by X-ray crystallography involves several stages: selection of the target; cloning, expression, purification, crystallization, collecting of diffraction data and determining of atomic positions (Smyth en Martin, 2000). The basis of X-ray crystallography is the interaction of matter in the crystalline state with X-rays. Since the wave-lengths of X-rays (0.1-10 nm) are of the same order of magnitude as of the interatomic distances within the crystal, the interaction results in the X-ray diffraction. Using X-ray crystallography, it has been possible to determine the three-dimensional structure of several ion channels. The voltage-gated K^+ channel KcsA from the bacterium *Streptomyces lividans*, for example, was crystallized and gave for the first time an ion channel structure with 3.2 Å resolution (Doyle et al., 1998). Some of its features provided the first views of ion conduction through the lipid bilayer (Doyle et al., 1998; Hucho en Weise, 2001). Crystallography has also allowed us to understand the molecular basis for several specific functions of ionic channels and revealed us crucial binding sites for controlling mechanism of conductance and selectivity. As an example, Doyle and colleagues, using the crystal structure of the bacterial K^+ channel, provided information about the selectivity of these channels. K^+ channels allow only one Na^+ ion to pass through for every 100 K^+ ions. Although a Na^+ ion has a smaller atomic radius than a K^+ ion, energetically speaking Na^+

ions cannot interact with the four pore-lining carbonyl oxygens that are held rigidly by the scaffolding of the K^+ channel protein (Doyle et al., 1998); since the energy barrier is higher for Na^+ than for K^+ ions, Na^+: K^+ selectivity of sodium channels is 10:1 (Grant, 2009 , Choe, 2002). This fact explains the high selectivity of ion channels. In addition, based on the detailed structure, some residues are the structural crucial factors that determine if a given channel is sensitive or insensitive to a certain toxin. For this reason, crystallography experiments may allow structure-based diagnosis and effective therapeutic agents development for life-threatening diseases based on this three-dimensional information (Jiang et al., 2020).

Isolated cells are one of the pivotal tools to investigate the function and expression of ion channels. Most ion channels are present in healthy or diseased cardiomyocytes (Zhao et al., 2018). The Langendorff system has been fundamental towards addressing questions in a wide range of mammalian heart species, ranging from mice, through rat and rabbit, dog, pig, primates and even human heart (Bell et al., 2011).

The Langendorff heart preparation involves the cannulation of the aorta (Fig. 4). The cannula is attached to the outflow of a reservoir with warm circulating water (Fig. 4e) to maintain the temperature of the heart at 37 °C. At the same time the heart is continuously gassed with oxygen containing 5% CO_2. The perfusion solution (buffer or enzymatic solution) is transported down the aorta through a calibrated peristaltic pump (Fig. 4b). This retrograde flow shuts the leaflets of the aortic valve so that the perfusion solution cannot enter the left ventricle and the perfusion solution is evacuated into the coronary arteries. After perfusing, the perfusate exits the coronary venous circulation via the coronary sinus and out of the open right atrium. Finally, the preparation allows the heart to be digested into individual cells. This approach provides highly reproducible preparations and uniform populations of isolated cardiac cells (Bell et al., 2011).

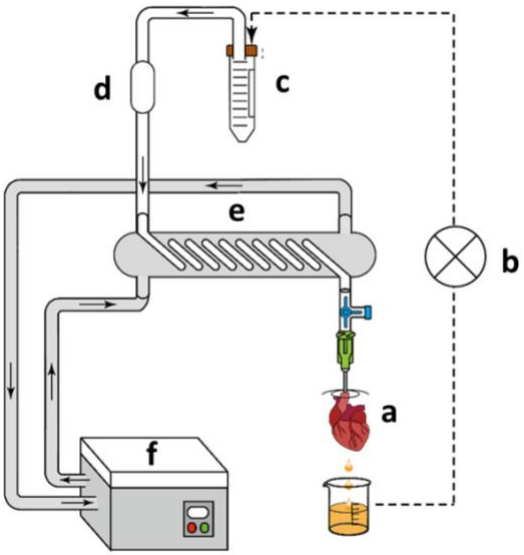

Fig. 4. Schematic Langendorff system. Myocardial perfusion is done via the coronary arteries that are filled in a retrograde manner. **a** Aortic cannula; **b** Peristaltic pump; **c** Perfusion fluid; **d** Oxygenation with 95% O_2 and 5% CO_2 tank; **e** Heat exchanger coil; **f** Water bath. The perfusion pressure (between 60 mm Hg and 80 mm Hg) or flow (between 4 mL/min and 5 mL/min) are kept constant. Arrows indicate the direction of flow (Li et al., 2020).

Intracellular recording methods imply measuring the membrane voltage or current by accessing the inner cell with an electrode, thus allowing signals to be recorded with a high signal-to-noise ratio. Nevertheless, intracellular methods are therefore rather invasive. In comparison, extracellular recording methods are non-invasive and allow multiple measurements, but sacrifices the accuracy needed to fully understand the properties of ion channels. Consequently, ion-channels are usually studied by intracellular recording methods, such as patch-clamp (Xie et al., 2012).

In the late 1970s, recordings of single channel currents flowing across the membrane were performed for the first time by Sakmann and Neher (Neher en Sakmann, 1976). They developed the patch-clamp technique and received the Nobel Prize in Physiology and Medicine in 1991 (The Nobel Prize in Physiology or Medicine, 1991).

Basic principle of the patch-clamp technique

Depending on the ion channels of interest, intra- and extra-cellular patch-clamp solutions must be prepared (Fig. 5I). Pharmacological activators or blockers of the channels of interest can be used to isolate the current of interest from the rest (contaminating currents). Cells are isolated using methods like the Langendorff perfusion (Figs. 4 and 9) and patch pipettes are fabricated following a given manufacturing protocol, as shown in section 4.2 *Pipette fabrication*.

In the patch-clamp technique, the cell membrane is electrically isolated from the surroundings with the glass pipette (Sakmann et al., 1981). For such experiments the steps from A to F have to be followed: **(A)** the pipette is attached to the membrane using a micromanipulator (Fig. 5, steps IV and V). **(B)** The pipette's resistance is monitored by applying a voltage step pulse (100 mV, duration depends on the sample rate) from a holding potential (0 mV). For example, if the amplitude of the membrane potential output pulse is 100 mV as mentioned above, which corresponds to 10 mV at the default gain of 10 V/mV, the resistance of the pipette is calculated from Ohm's Law, thus obtaining 10 mV/1 nA = 10 MΩ. **(C)** When the bath resistance doubles, slight suction is applied with a syringe via a hydraulic pressure system connected to the pipette holder. The pressure in the tubing (in millibars) is then given approximately by: Pressure (mbar) ≈ -70*x + 350. For example, depressing the syringe to x= 4 cc = 70 mbar of pressure. One of the most important aspects in patch-clamp recordings is to decrease the electric background noise of the experiment to a level several times below the electric current generated by the flow of ions through an ion channel.

Successful seal formation (or gigaseal) is indicated by a decrease of the current amplitude evoked by the applied voltage pulse (current is approaching zero). **(D)** *Cell-attached* configuration is established once a stable gigaseal has been achieved (bath resistance > 1 GΩ). From this, **(E)** *whole-cell* configuration can be established by rupturing the membrane through a ZAP pulse by the MultiClamp 700B Commander and/or other techniques (Fig 5, steps. V to VIII). Zap function is an alternative to apply a large, brief voltage pulse to the electrode when in V-Clamp mode, to facilitate breaking into a cell for whole-cell recording.

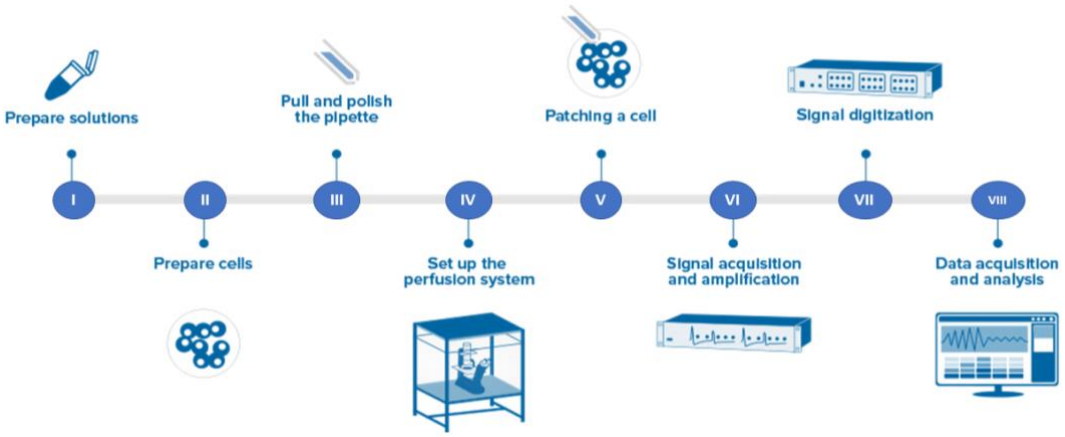

Fig. 5. Schematic diagram for a patch-clamp stimulation. **I** Solutions; **II** Cell lines; **III** Micropipette design; **IV** Vibration dampening, electrical shielding, microscope, micromanipulators, headstage, holder; **V** Procedure patching a cell; **VI** Amplifier; **VII** Digitizer; **VIII** Software.

For patch-clamp recordings, different configurations can be achieved: cell-attached, whole-cell, inside-out and outside-out (Fig. 7e) (Sakmann et al., 1981). The first configuration is necessary to achieve the others, the second was previously explained; here, the total current passing through all the channels, of the same type, can be measured. By contrast, in inside-out and outside-out patches, only currents through channels contained in the patch are measured.

From *whole-cell* configuration, **(F)** the simplest stimulation protocol is to clamp the cell at a 'holding' level for a few tenths of seconds and then move to new stimulus. The membrane is then returned to the original holding, before moving to another new pulse. The stimulus and the collection of a long series of amplified data (Fig. 5VI) (which is most conveniently presented by superimposing upon each other the series of changes in response to changes in the stimulus away from the holding) depend on the recording mode: *voltage-clamp* or *current-clamp* (Fig 6). The analog responses are then digitized so that the signals can be analyzed (Fig. 5VII, VIII).

Voltage-clamp mode: When voltage-clamp recordings are performed, current flowing across the membrane is recorded as a function of the input voltage through voltage steps

(protocols), as Fig. 6a shows (Boron en Boulpaep, 2012). Once high-quality seals are established and background signals are minimized, specific membrane conductance can be recorded. Typical shapes of the peak of each current plotted against the voltage commanded (I–V curves) are shown in Fig. 7b, 7d. The slope of this curve is the single-channel conductance. In response to depolarization, the channel activates and current flow will be outward (positive) or inward (negative), depending on whether V_m is greater than or less than V_{rev}.

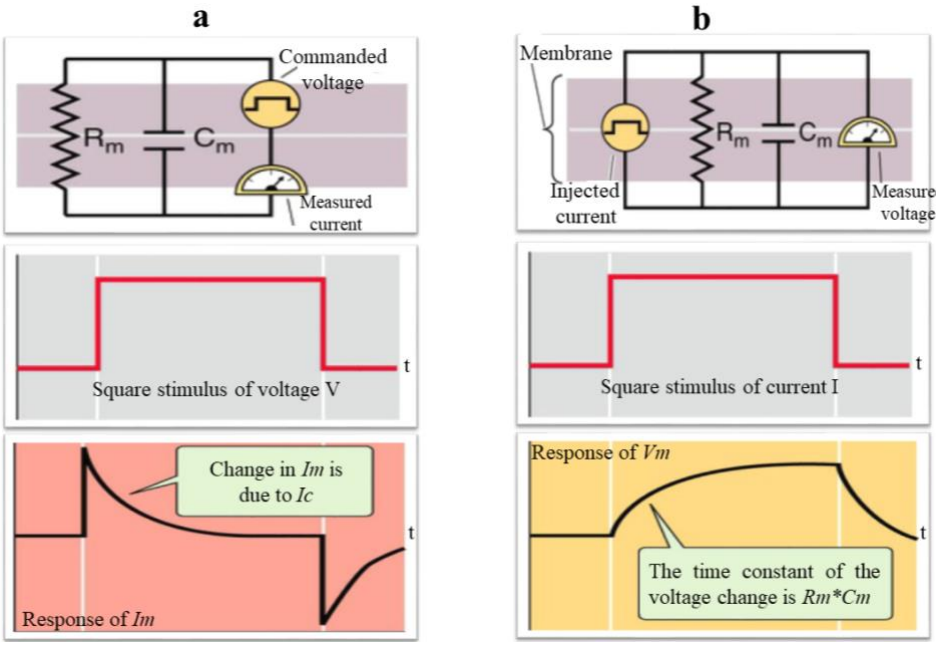

Fig. 6. Voltage and current responses caused by the presence of a membrane capacitance. **a** Voltage-clamp recording; **b** Current-clamp mode. The response of the cell to an electrical clamp stimulus responds to the detailed description in chapter 1. (See 1.2 *Describing the cell as an electrical circuit*) (Boron en Boulpaep, 2012).

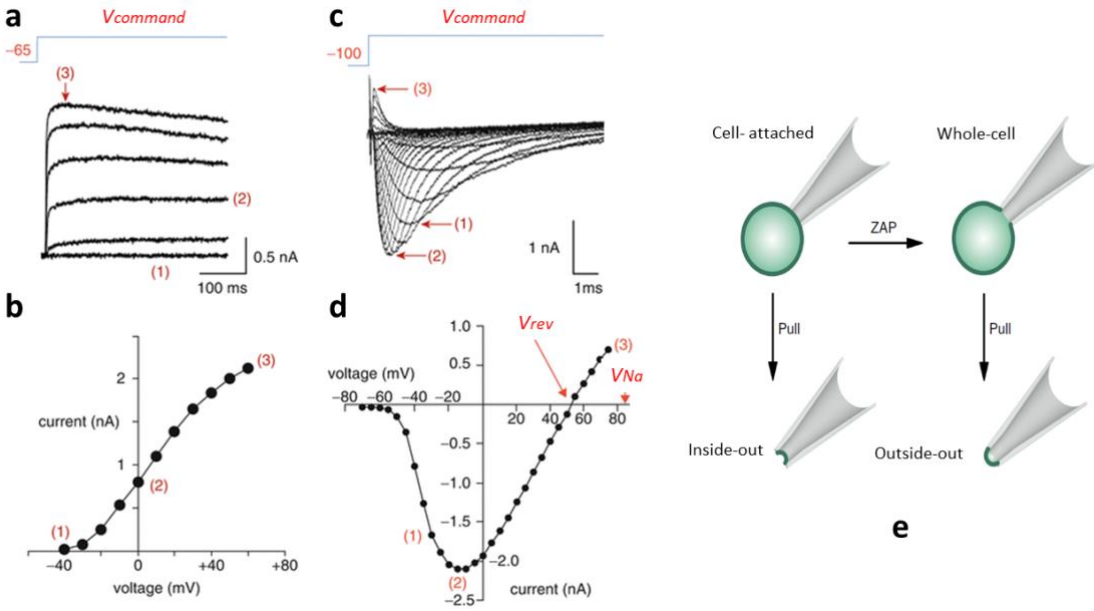

Fig. 7. Current-voltage curves of voltage-gated K^+ and voltage-gated Na^+. currents. **a** and **c** show overlapped current records over a range of pulse potentials for K^+ and Na^+. currents, respectively, which is comparable to Fig 3a. In the figure only one pulse is shown; The relationships between pulse potentials and peak currents (I-V curves) are shown in panels **b** for K^+ (arterial smooth muscle cell) and **d** Na^+ (rat ventricular myocyte). Na^+ current shows a clear reversal (V_{rev}) at about +55 mV. The red numbers (1), (2) and (3) are

used to show the correspondence between the peak of each current versus time curve in the I-V curve (Synthase, 2013); **e** Patch-clamp can be made in three different configurations: cell-attached, whole-cell, inside-out and outside-out (Chen et al., 2017).

Current-clamp mode: The membrane voltage in a cell can be studied using current-clamp experiments. In this mode, changes in the membrane potential are recorded as a function of the size of currents injected into the cell (Fig. 6b) (Boron en Boulpaep, 2012). These recordings are useful to examine the AP, V_{Nernst}, and dynamic changes of the V_m (Chen et al., 2017).

As mentioned above, the high resistance of the gigaseal in patch-clamp recordings, dramatically reduce the background noise levels. The total root mean square (rms) noise of a patch-clamp recording is the square root of the sum of the individual squared rms noise sources. Background noise arises from a variety of different sources: the Johnson noise of the membrane-seal combination, the "shot noise" from ions crossing the membrane, intrinsic noise in the pipette, noise in the current-to-voltage converter, capacitances transient (for more complete summaries of the noise, the reader is urged to read the excellent work by (Sakmann et al., 1981)). The largest individual noise source can often dominate the total noise and limits the time resolution of the recordings. Thus, different techniques have been developed in order to reduce these types of noise sources, many of which have previously been described (Levis en Rae, 1998; Sakmann et al., 1981; Sigworth, 1983). Some of the most important techniques are the series compensation (*Rs* compensation) produced by the pipette, the capacitance transient cancellation and whole-cell compensations. These potentially contributing noise sources must be electronically reduced. Therefore, it is important to note that the success of a good record depends on the quality and resolution of the equipment used in the setup and the skills of the experimenter.

The movements of ions can be measured through a single channel protein as well. By sealing an electrode around a small area of membrane, or by incorporating a channel protein into a planar lipid bilayer. Single channel traces represent changes in current upon conformational changes of a single ion channel protein catalytic ('open') and non-transporting ('closed') states, this is called *gating*, as explained by H-H. The size of the currents can be plotted against the clamping voltage to produce an I-V curve (Tester, 1997). When the channel is in a close state, the current amplitude is very low, near to 0 pA. The amplitudes of open-channel currents depend on the amplifier calibration settings (e.g. main amplitudes of 1.9 pA can be seen) (Mortensen en Smart, 2007). Other figures can illustrate the probability of finding the channel in the 'open', or conducting, state. The major problem to measure single-channel currents is the size of the background noise signal (Tester, 1997). For obtaining the highest resolution of channel opening and closing events, low-noise recordings, coupled with a minimal filtering frequency, are required (Mortensen en Smart, 2007). Noise components are the same that arise in patch-clamp experiments (Levis en Rae, 1998). Thus, the noise and the extent of filtering should be kept to a

minimum (e.g. noise of 0.057 pA RMS in a 5-kHz bandwidth) (James L. Rae; Richard A. Levis, 1992). In our Biophysics and PHYSIS laboratory, the electronic components also possessed sufficient resolution to be able to detect single-channel currents of a few picoamperes, for long-term and low-noise single-channel recordings.

Chapter 5
Cardiac cells

Isolated perfused heart preparations serve as model for studying fundamental mechanisms underlying cardiac physiology and pathophysiology, as well as identifying potential therapeutic targets. This chapter describes the isolation of cardiomyocytes from adult mouse hearts. The Langendorff technique was used for the isolation of these muscle cells. Under optimum conditions, isolated cardiomyocytes showed intact morphology, with the final suspension containing about 80% intact cells. These cells can be used not only for patch-clamp experiments, but for a variety of physiological, biomechanical and biochemical assays.

5.1. Introduction

The heart is a muscular pump with the primary function of maintaining pulmonary and systemic blood flowing to support all organs with sufficient oxygen and nutrients. The main contractile portion of the heart is composed of cardiac cells, also called cardiomyocytes (CM). Adult ventricular CM are approximately cylindrical (~100×10 μm) and binucleated, having an extensive t-tubule network and a characteristic intercalated disc structure (Fig. 8a-d), through which an AP can spread with high speed and low resistance (Fig. 8e-h). Cardiac ion channels are located in three major functional and structural entities: the intercalated disks (ID), the lateral sarcolemma, and the Excitation coupling (E-C) domains (Balse et al., 2012).

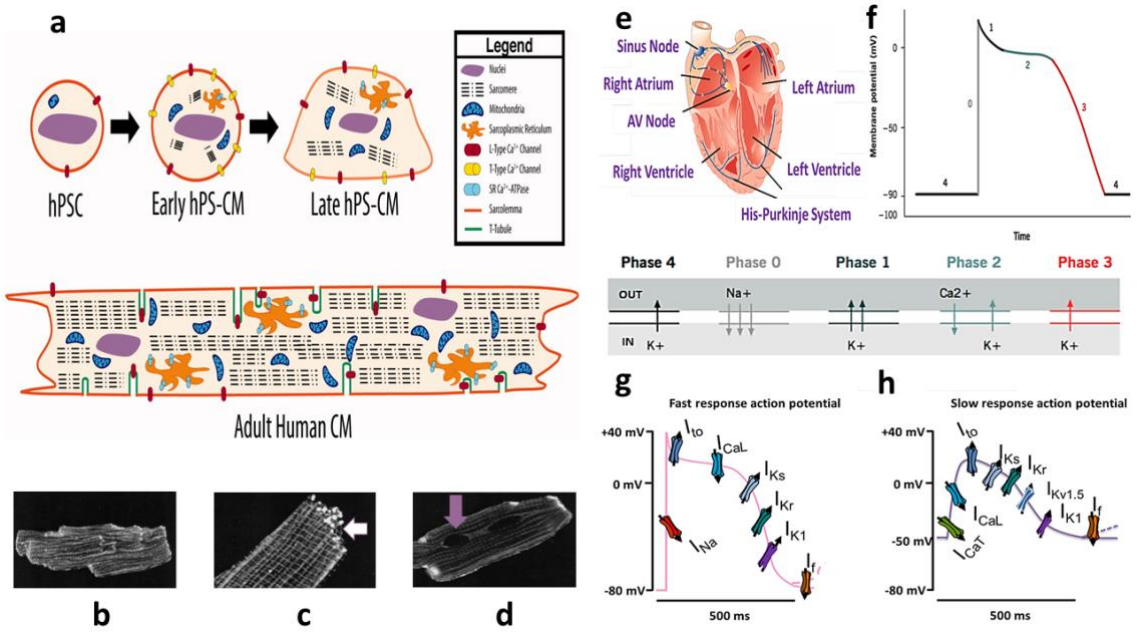

Fig. 8. A comparison of early human pluripotent stem cell-derived cardiomyocytes (hPS-CM), late hPS-CM and adult CM morphology. **a** Note that adult CM are far larger, with multiple nuclei, large sarcomeric area, and large numbers of mitochondria (Robertson et al., 2013); **b** The intercalated disks as well as weak striated staining of the transverse tubules is observed; **c** Showing the region of the intercalated disk; **d** One nucleus is indicated by the arrow, in a binucleated CM (Maier et al., 2002); **e** Cardiac components involved in conduction of electrical impulses from the sinus node through the His-Purkinje system; **f** AP comprises phase 0 through phase 4. Some channels may conduct in an inward or outward direction, depending on the membrane voltage at any given time point of the electrical cycle. AP duration (APD) is approximately 200 ms (Grant, 2009; Greg Ikonnikov and Dominique Yelle, 2018); **g** Typical morphology of a cardiac AP in fast-response tissues (i.e., atrial and ventricular myocardium and Purkinje fibres). Each AP comprises phase 0 through phase 4; **h** A cardiac AP in slow-response tissue (i.e., the SA node and AV node) (Huang et al., 2017).

Cardiovascular electrophysiology has been developed in small mammals (e.g. rats, rabbits, and cats), but also in large (e.g. non-human primates, dogs, sheep, and pigs) and even in non-mammalian vertebrates (e.g. newts and zebrafish). However, due to the high genetic similarity to the human heart and the relative ease of genetic manipulation, mice and rats are the most widely used animal models for cardiac cellular physiology, pathology, drug toxicity screening, and intervention in the biological and medical research fields (Liu et al., 2019).

Cardiomyocytes were first isolated from embryonic chick hearts (Burrows, 1910). However, isolating cardiac cells is difficult because they are firmly adhered to each other by intercalated disks and the extracellular matrix network in the heart. Moreover, CM are susceptible to hypoxia, physiological deterioration, mechanical perturbations, nutrient availability, pH, temperature changes, ionic fluctuations, and particularly vulnerable to enzymatic digestion. Therefore, cells must be newly isolated for each individual experiment (Ackers-Johnson et al., 2016; Ferdinandy et al., 2007). A highly reproducible procedure that guarantees a great quality of the CM is the Langendorff technique of isolated heart perfusion, as shown in Fig. 4 and, our results implementing this technique are shown in Fig. 9. Our goals proposed isolated cardiac cells as the model to understanding the effects of toxins from the venom gland of the spider *Pamphobeteus verdolaga*.

5.2. A highly reproducible method for isolating viable cardiomyocytes murine cells from the adult mouse heart

Animals

All experimental procedures involving animals in this research were approved by the institutional ethics committee for animal care of the University of Antioquia. Experiments were carried out on isolated cells from male Swiss Webster mice weighing 20–26 g, obtained from the vivarium of the University of Antioquia. Animals were handled gently to minimize stress that may affect the neuro-humoral state of the cells. All solutions were filtered with 0.22 µm nitrocellulose filters. All tools were cleaned by surface sterilization with 75% ethanol. A schematic overview of the myocyte isolation procedure is shown in Fig. 9.

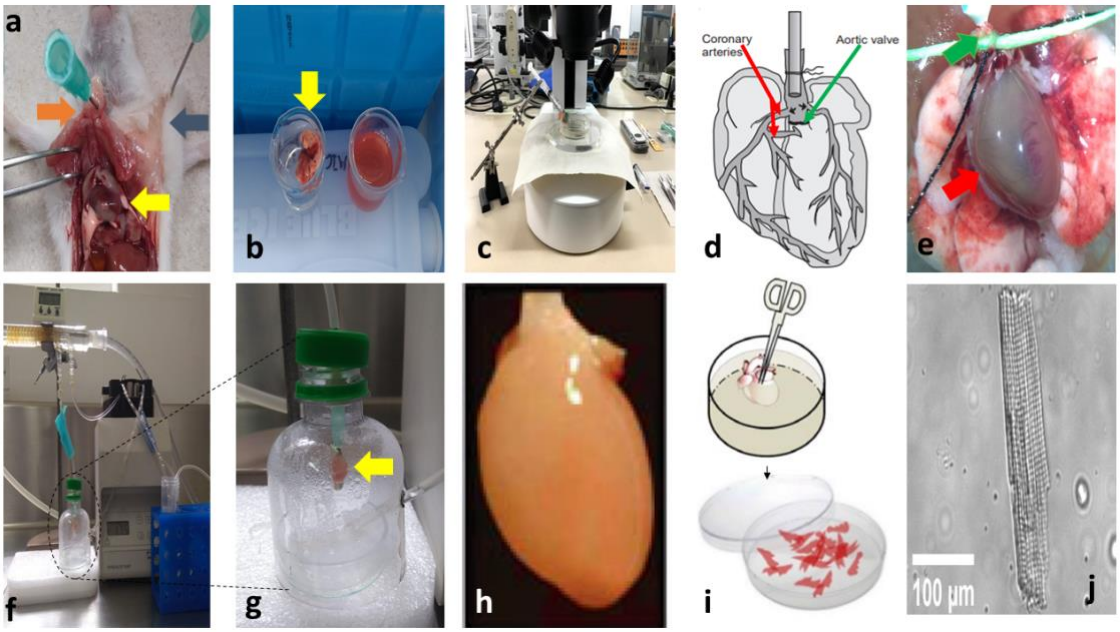

Fig. 9. Isolation of cardiac tissue from an adult mouse. **a** Chest cavity were opened to fully expose the heart; The yellow arrow shows the heart, the orange: the thoracic cavity, the gray: skin; **b** Heart was transferred twice into an ice-cold Ca^{2+}- free Tyrode's solution supplemented with heparin; **c** Set up for heart cannulation; **d** Proper cannulation. Placing the cannula too deep in the aorta and through the aortic valve will prevent adequate perfusion of the coronaries and cardiomyocyte isolation will not be successful; **e** Higher magnification figure illustrates an isolated heart secured to a cannula tip with two threads tied around the aorta. The lungs are shown; **f** Langendorff system used for heart perfusion; **g** The heart was covered with a chamber to conserve heat (yellow arrow). **h** Following perfusion with the digestion buffer, the heart became progressively edematous and appeared pale and flaccid; **i** Following enzymatic digestion, cardiomyocytes were dissociated by teasing apart the tissue with sterile-opposed forceps followed by gently pipetting the suspension with a plastic transfer pipette; **j** Overview of a freshly isolated cardiomyocyte in 20x. Scale bar=100 µm.

Isolation of cardiomyocytes

Preparation of the perfusion apparatus (Langendorff System, Fig. 4) ● TIMING 20 min: Before starting to remove the heart from the animal, the perfusion system was prepared. The Langendorff perfusion system should be flushed with sterile water (15 min). The temperature of the water circulator must be adjusted to achieve a perfused temperature of 37°C (measured at the

cannula tip). A tube A with 50 ml of Ca^{2+}- free Tyrode's solution (Ca^{2+}-free modified Tyrode solution (in mM): NaCl 135, KCl 5,4, $MgCl_2$ 1, Glucose 10, HEPES 10, NaH_2PO_4 0.33, with adjusted pH 7.2 (NaOH)), recirculated through the system for 5 min at constant perfusion flow rate of 4.5 ml/min. This helped to remove any residual air bubbles and distilled water in the system. The solution A (Tyrode pH 7.2) with blood was discarded in the collector beaker.

Dissection of the heart and cannulation ● TIMING < 15 min: The animal is weighed prior to sacrifice. The time of digestion was dictated by the weight of the animal. Once the animal was successfully anesthetized, it was sacrificed through cervical dislocation and transferred to a surgery area to be fixed on a dissecting board. A small incision in the stomach for entrance of the scissors was made to proceed with a cut to carefully separate the skin from the underlying musculature. The thoracic cavity was then opened by cutting through the diaphragm and the costal cartilages at their point of union on both sides until reaching the armpit. Once the heart was exposed pulmonary vessels and the aorta were identified, it was gently pulled up using fine curved head forceps. The heart was rapidly removed (Fig. 9a). It is crucial to leave as much of the ascending aorta as possible, including the lungs, to facilitate cannulation. Finally, the heart was rapidly immersed twice in cold Tyrode solution with heparin, until it was cleansed from blood excess (Fig. 9b).

As shown in Fig. 9e, the aorta was placed into the cannula. This step ensure that the coronary arteries were filled with the enzyme solution. To make the cannulation easier, a stereo microscope is used (Fig. 9c). The lungs were positioned concavely towards the observer in order to anatomically locate the heart and to be able to adequately visualize the perfusion of the coronary arteries. After the aorta was cannulated and strongly sutured, the adequacy of the perfusion was confirmed when the coronary arteries were filled with the solution within the syringe (Tyrode with heparin). Finally, the lungs were cut and the cannula was cautiously removed from the syringe and carefully located in the Langendorff system to avoid introducing new air bubbles.

Enzymatic Tissue Digestion ● TIMING 24 min (Fig. 9f-g): In this stage, all solutions were bubbled with 95% O_2 and 5% CO_2. In addition, temperature, pH, 95% O_2 and 5% CO_2 flow, perfusion volume, were constantly monitored.

First, the heart was perfused with the resulting solution remaining in tube A for 6 min until the blood was cleared, then perfusion with the enzymatic solution starts, 10 mL of solution B (Ca^{2+}-free Tyrode's solution with pH 8,0) supplemented with 1 mg/mL collagenase (type 2; Worthington, Lakewood, NJ) and 0.1 mg/mL protease (type XIV; Sigma, St. Louis, MO). Here the solution was recycled to the reservoir B by pumping. Following time of perfusion with the digestion buffer, the heart became progressively pale and soft to the touch (Fig. 9h).

Post-perfusion Digestion ● TIMING 1-3 min (Fig. 9i): The heart was placed in a petri dish. Because the atrial cardiac potential is different from the ventricular one (Figs. 8g and h), the ventricles were cut and softly separated from the atrium. Only the ventricles were transferred to a separate petri box which contained warm Ca^{2+}-free modified Tyrode solution and triturated into small pieces with grippers. In this step, it was crucial to reduce mechanical pressure during trituration.

Chapter 6
Ca^{2+} currents in cardiac myocytes

Cell excitability is central to cardiac physiology. Many cardiac ion currents have been identified and described. VGCC converting depolarization of the cell membrane to an influx of Ca^{2+} that regulate excitation–contraction coupling, secretion, neurotransmission, and other intracellular regulatory events. Malfunctioning of these channels has been implicated in human diseases. Therefore, these channels have engendered very high interest as future molecular targets. In the present chapter, we present a protocol detailing about how to implement the whole-cell patch-clamp technique to characterize Ca^{2+} currents from cardiac myocytes. The experiments were performed at room temperature. Our results prove feasibility of patch-clamp recordings on cardiomyocytes and their potential use for in-depth toxin evaluation, as well as for diagnosis and pharmacology tests for cardiac channelopathy patients.

6.1. Introduction

As sketched in Fig. 8f-h VGCC are protein-complexes that activate at negative voltages at the beginning of the systolic depolarization and importantly contribute to this phase by supplying inward current responsible for the initiation and propagation of the cardiac AP. Their principal α subunit (212–250 kDa) consists of four homologous domains (DI–DIV) (Fig. 10) (Jiang et al., 2020; Maier et al., 2002; Reuter, 2013). Each domain contains six transmembrane α-helices (segments S1-S6) with a membrane-reentrant loop between them (the transmembrane pore, TP) and cytoplasmic regions at the N and C terminal ends. S1-S4 form the voltage sensor domain (VSD). The voltage sensor, S4 segment in VSD, consist of repeated motifs of a positively charged residue, usually arginine, followed by two hydrophobic residues. The inactivation gate is the loop linker between DIII-S6 and DIV-S1 and it contains the important hydrophobic triad.

Ca^{2+} channels have a single family of auxiliary α2δ, β, and γ subunits, that can bind to the α subunit either non-covalently or through a disulfide bond. These accessory subunits play important roles in the regulation of both the biophysical properties and trafficking of Ca_v channels. In CMs the fully functional $Ca_v1.2$ channels that contain $Ca_v\alpha$, $Ca_v\beta$, and $Ca_v\alpha2\delta$ subunits are primary macromolecular complexes (Rougier en Abriel, 2016).

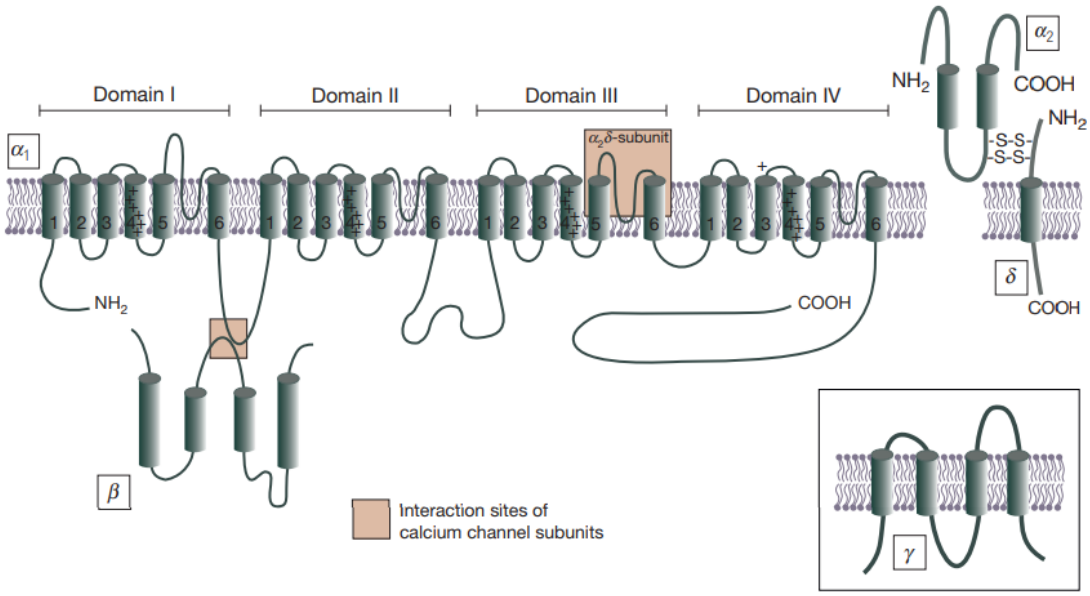

Fig. 10. Ca^{2+} channel structure and organization. The subunit composition consists of the pore-forming α subunit with its four homologous domains (I-IV) and the auxiliary α2δ, β, and γ (inset) subunits. Predicted alpha helices are depicted as cylinders (Reuter, 2013).

Six different types of voltage-dependent Ca^{2+} channels have been identified: L-, N-, P-, Q-, R- and T-type. The mammalian isoforms of VGCC share high sequence homology in the transmembrane and extracellular domains but are expressed in different tissues. The gating properties of these isoforms vary, as does their sensitivity to neurotoxins and blockers. Four α1-subunits ($Ca_v1.1$, $Ca_v1.2$ $Ca_v1.3$, and $Ca_v1.4$) have been cloned for the L- type Ca^{2+} channel ("L" stands for long-lasting of activation). They are activated from about -30 mV and are highly sensitive to dihydropyridines (DHP) Ca^{2+} channels modulators (Mesirca et al., 2015). $Ca_v1.2$ and $Ca_v1.3$ are expressed in neurons, in cells from the neuroendocrine and cardiovascular systems. $Ca_v1.1$ is expressed in the skeletal muscle. $Ca_v1.4$ expression is major in the retina, spinal cord and immune cells. Three Ca_v2 channels have been found ($Ca_v2.1$ or P-/Q-type (expressed in Purkinje neurons in the cerebellum / Cerebellar granule cells), $Ca_v2.2$ or N-type (throughout the brain and peripheral nervous system), and $Ca_v2.3$ or R-type channels (cerebellar granule cells, other neurons)) (Senatore et al., 2016). Three genes encoding for T-type channels (transient opening Ca^{2+} channels), activated at −50 mV, have been named $Ca_v3.1$, $Ca_v3.2$, and $Ca_v3.3$. $Ca_v3.2$ is expressed in embryonic heart tissue. In adult, $Ca_v3.1$ expression is higher than $Ca_v3.2$. $Ca_v3.3$ is not present in the heart. T-type channels are almost insensible to DHP (Mesirca et al., 2015).

Properties of the Ca^{2+} current in cardiac myocytes have been determined previously (Table 1) (Yamakage en Namiki, 2002).

Table 1. Electrophysiological classification and characteristics of cardiac VGCC (Yamakage en Namiki, 2002).

Parameter	L-type	T-type
Voltage dependence	High voltage activated	Low voltage activated
Threshold activation (mV)	-30 ~ -10	-70
Inactivation range (mV)	-60 ~ -10	-100 ~ -60
Rate of inactivation (decay time constant) (msec)	>500	20-50
Single channel conductance (pS)	25	8
Antagonists/blockers	DHP= dihydropyridine; PAA=phenylalkylamine; BTZ=benzothiazepine	Mibefradil; ω-Aga IIIA=agatoxin IIIA

For more complete summaries of the major quantitative data for voltage dependence of activation and inactivation, single-channel conductance of calcium currents of several cells, the reader is urged to read these excellent documents (Yamakage en Namiki, 2002; Nuss en Marban, 1994; Catterall et al., 2021; Niwa et al., 2004). In the present chapter, we present a protocol detailing about how to implement the whole-cell patch-clamp technique to characterize the kinetics of Ca^{2+} currents from cardiac myocytes.

6.2. Implementation of patch-clamp technique to the study of Ca^{2+} currents

Cleaning the glass capillaries ● **TIMING 4 h:** This is the most important step for patch-clamp experiments. When the pipette is dirty, the seal cannot be achieved or a "gunk-seal" can be established and the whole-cell configuration is difficult to obtain (Kolb et al., 2016). If pipettes need to be used for more than a few hours, they should be cleaned before using by soaking them in ultra-pure water for two hours and then fully heat drying in an oven (about 2 h).

When a capillary was completely dry, positive pressure was applied inside it using a holder that is connected to a syringe (Fig. 11). The positive pressure was repeated at least 6 times to ensure there are no particles contaminating the inner (1 min). Two pipettes were immediately fabricated with a clean capillary.

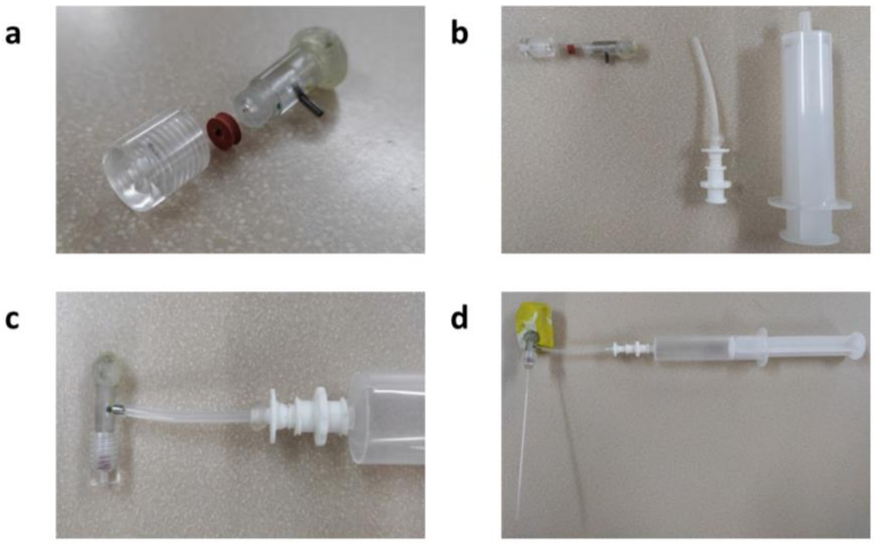

Fig. 101. System designed for cleaning patch-clamp pipettes. **a** Holder without Silver wire, with cone washer, suction tube and with the pin cap close by silicone; **b** Holder with the silicone tubing and a syringe; **c** Assembled Holder; **d** The holder is mounted on plasticine to get stability, then the capillary is correctly located inside the pipette cap and later the positive pressures is applied through the suction tube with the syringe. Always the whole system is kept clean and dry**.**

Pipette fabrication

Patch pipettes were made in a two-stage process: pulling a capillary and heat polishing of the pipette tip.

First step-pulling ● TIMING 1–3 min per capillary: Patch pipettes were pulled from Schott glass capillary with length: 10 cm, outside diameter of 1.65 mm and inside of 1.20 mm. Schott 8250 composition (today's equivalent of Corning's old 7052 glass) provides good electrical properties (Single Barrel Capillary Glass Without Microfilament for Patch Clamp). Optimal pipette geometry and pipette resistance were essential to the formation of gigaseals. The optimal geometry of patch pipettes for patch-clamp is shown in Figs. 10f and 10h. The pipettes were pulled in two stages by a horizontal microelectrode puller (P-1000, World Precision Instruments (WPI); Fig. 12a-b). To obtain large numbers of pipettes with similar properties it is advisable to use fixed settings for the two stages (Fig. 12c). Table 2 provides some basic guidelines to configure the sequence that allowed us to design our pipettes. Finding the right sequence to get the desired glass pipette requires experimentation.

Table 2. Effect different parameters on pre-pulled pipette shapes and dimensions (Manual).

Parameter	Increase (↑)	Decrease (↓)
Heat	Longer Taper	Shorter Taper
Force	Smaller Tips, Longer Taper	Larger Tips, Shorter Taper
Distance	Smaller Tips	Larger Tips
Delay	Shorter Taper	Longer Taper

The glass capillary was mounted onto the puller as described in the Figs. 12b and 12c. In the step one pre-pull the capillary is thinned to obtain a minimum diameter of 200 µm (Fig. 12e). The capillary is then re-centered with respect to the heating coil and in the second step the thinned part breaks, producing two pipettes. Our aim was to obtain tips between 3 and 5 µm (Fig. 12. f-h).

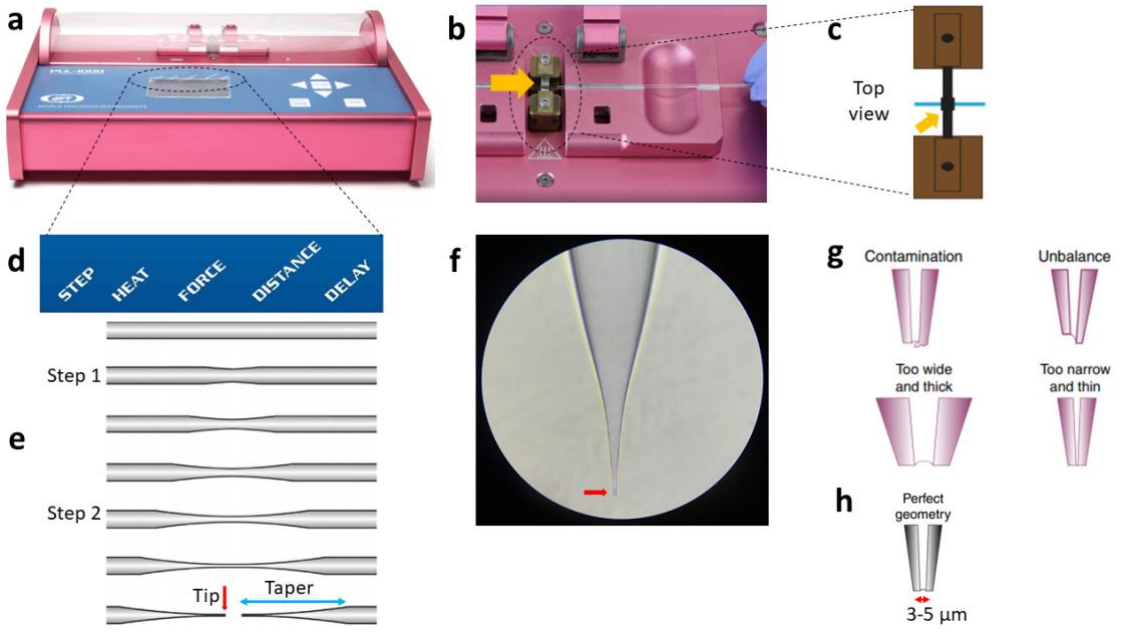

Fig. 12 Setup used for the fabrication of optimal patch pipette. **a** Pipette puller; **b, c** Correctly manufacturer's protocol for mounting the glass capillary. The yellow arrow shows the heating filament; **d** Different parameters that were modified for getting the pipettes shapes and dimensions; **e** Pipettes after each individual pulling sequence are shown; **f** Ideal pipette seen in the vision field of the objective microscope lens of the fire polisher before polishing. The opening diameter, sharpness and geometry were inspected. The red arrow shows the pipette Tip. It was verified for imperfections. The vision field of the 20× objective microscope lens; **g** Failed pipettes process are shown. Pipettes may be contaminated or unbalanced with glass. Suboptimal pulling conditions can result in pipette tips that are too wide or too narrow. These pipettes were discarded; **h** An example of a pipette with perfect geometry (Chen et al., 2017).

Second step- heat polishing ● TIMING 2 min per pipette: Polishing of the glass wall at the pipette tip was done on a microforge (MF 200-1, WPI) (Fig. 13b). We observe this step using a compound microscope (Fig. 13a). The heat was supplied by a V-shaped platinum-iridium filament (Fig. 13c-e). The tip of the pipette was brought to within 10-30 µm of the filament for a few seconds. The filament was heated to a red glow (Fig. 13e).

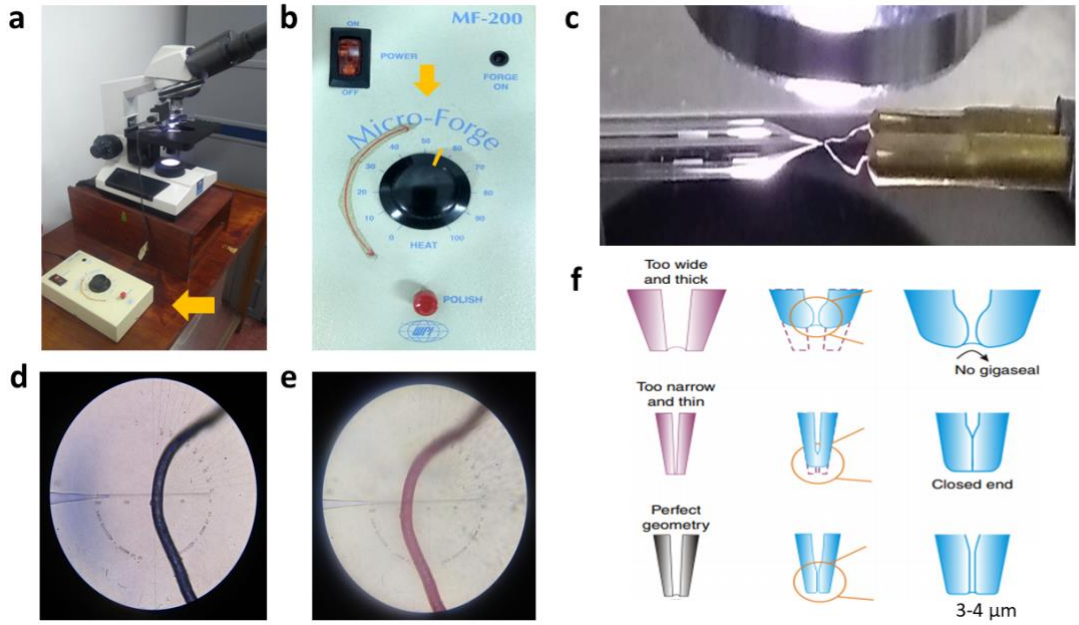

Fig. 113. Fire-polishing of patch-clamp pipettes. **a** Microscope; **b** Micro-Forge. The Heat knob was set to a maximum intensity of 55 in an arbitrary scale (yellow line); **c** Fire polisher is shown; **d** V-shaped platinum-iridium filament before polishing; **e** Red filament during polishing; **f** Before polishing (left column) and after polishing (middle and right columns). Pipettes that are too wide and thick can result in no gigaseal formation. Closed-end tip pipettes are produced by overpolishing. Finally, pipette with ideal geometry after polishing is shown. Only pipettes with perfect geometries were used (Chen et al., 2017).

Recording solutions

The pipette solution contained (in mM): HEPES 11, EGTA 10, CsCl 125, MgATP 5 (pH 7.1 with CsOH) and the external solution (bath solution) was (in mM): Tetraethylammonium (TEA) 140, $MgCl_2$ 1, CsCl 6, $CaCl_2$ 1, HEPES 10, Glucose 10 (pH 7.4 with CsOH). To minimize and/or eliminate other ionic components, a selective channel blocker were incorporated in the external solution because in the extracellular mouth the pore is where this toxin bind (Catterall, 1995). To block potassium currents CsCl was used in both the internal and external solutions (IUPHAR/BPS Guide to PHARMACOLOGY, 2022). In addition, TEA is a K^+ channel blocker for a diverse group of K^+ channels. To eliminate Ca^{2+} currents and Na^+ currents, electrical protocol was implemented. The solutions were cleaned by passing it through a cellulose filter two times. Aliquots of 2 mL in conical tubes were stored at 4 °C for up to 2–4 weeks.

Patch-clamp recordings

Preparation of the experimental chamber ● TIMING 5–15 min: Once the cells were isolated as explained in Chapter 5 they were inspected under microscope (20× objective lens) and those with defined membranes, well adhered to the coverslip, square, small were chosen to record currents.

Gigaseal formation ● TIMING 5–10 min (Chapter 2; Patch-clamp technique: Basic Principle): Using a micro Filler connected to a syringe which contains 2 mL of internal solution,

a clean pipette was filled with this solution avoiding bubbles and then, was mounted onto the headstage of the patch-clamp setup. The angle of the headstage should be close to 30°. Then, the pipette tip was moved into the bath solution and placed it in the middle of the visual field. The offset voltage of the pipette was adjusted to 0 mV. Then, the steps explained in the Basic principle of patch-clamp technique **(A-E)** were applied to establish whole-cell configuration (Fig. 7e Based on our experience by syringe or ZAP function: a conventional method for rupturing a membrane patch to go to whole-cell). Suction pulse applied via the mouthpiece was not used because of the risk of coronavirus SARS-Cov-2 infection.

Recordings in whole-cell configuration, voltage-clamp mode ● TIMING 1–5 min (Chapter 2; Patch-clamp technique: voltage-clamp mode): After establishing the whole-cell recording configuration, the following records were made:

RECORDINGS A: Studying kinetics of activation of Ca^{2+} currents:

i. Current changes in response to different square pulses were recorded. Current time curve (I-T). The activation of the total Ca^{2+} currents was studied with voltage steps from -50 to +60 mV in 10 mV increments from a holding potential of -50 mV for 100 ms (Ca_v protocol). Representative stimulation protocol traces are shown in Fig. 14. The signal that resulted from this stimulation was plotted in terms of time following Fig. 7c.

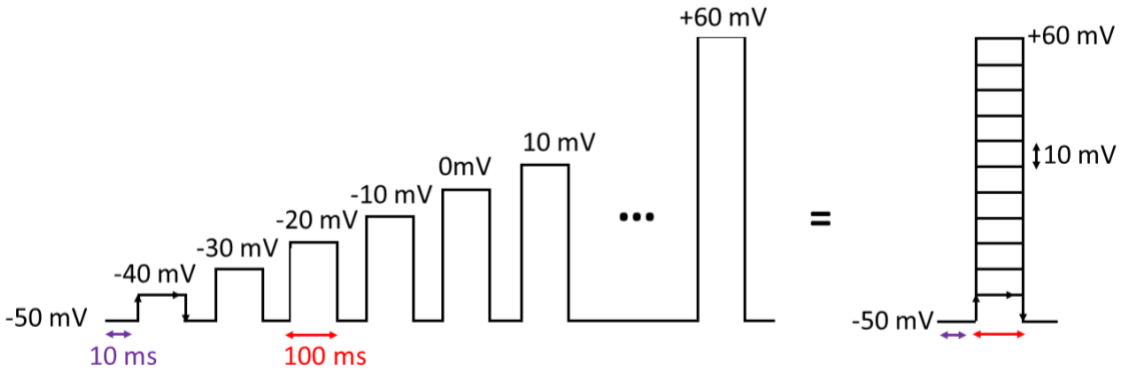

Fig. 14. Patch-clamp protocol to stimulate Ca^{2+} channels. On the left the expanded protocol is shown and on the right the superposition of the pulses is shown as is typical of seeing them in research articles.

To examine effects of Nifedipine on calcium currents, Ca_v protocol was applied without the presence of Nidedipine in the bath solution (control current) and after treatment with Nifedipine (5 and 13 µM). Thus, the current was plotted in terms of the time.

L- type or T-type Ca^{2+} currents can be calculated by the electronic circuitry provided with the amplifier and the Clampfit program of the Clampex. Mathematically, the algebraic sum of Ca^{2+} currents can be expressed as:

$$I_{\text{total}} = I_{\text{L- type } Ca^{2+}} + I_{\text{Total Nifedipine}}$$

where I_{total} is called the control current.

RECORDINGS B: Studying ionic current voltage-dependence:

Current-voltage relationships (I-V) allow summarizing the behavior of voltage-gated ion channels (Fig. 7c). Parameters such as: reversal potential, ionic dependence/selectivity, voltage dependence, activation threshold, slope, as well as the overall quality of patch-clamp, can be easily derived from these curves. There are two factors that determine the flow of current through an open channel, firstly the conductance and second, the reversal potential (V_{ion}).

The currents evoked at a given potential were plotted using a variety of considerations:

i. Peak and steady-state IV curve

Peak currents were measured as the largest current obtained when a voltage step was applied. If a current had transient peak current amplitude, the maximum current was determined by the software Clampfit and these values were plotted against voltage. If the Ca^{2+} currents did not exhibit this defined peak, steady state values were used, typically were recorded at the end of a voltage step.

These curves were fitted by a single Boltzmann function. The ability to measure Ca^{2+} currents critically depends on fully compensating for series resistance of the pipette (*R*s). *R*s compensation was usually compensated to 50% in order to minimize voltage errors. The P/4 protocol was used to subtract leakage currents. The automatic Cp fast and slow, whole-cell compensation were implemented to reduce capacitances. Samples were recorded at 10 kHz, filtered at 5 kHz (low-pass filter), and stored for offline analysis.

Data analysis

Recordings were analyzed with Clampfit 10.0.5 (Molecular Devices, USA) and ORIGIN Pro2019 software (Origin Lab Corporation, Northampton, MA, USA). Results were expressed as means ±S.E.M. Statistical differences were evaluated by paired t-tests and considered significant at $P < 0.05$.

Chapter 7
K^+ currents in cardiac myocytes

K^+ channels are by far the largest and most diverse of the ion channels. These channels allow K^+ flux and as sketched in Fig. 8f-h (phases 1 - 4), are essential for regulating cardiac muscle excitability by controlling AP duration and frequency. The behavior of VGPC can be modified by intracellular processes, toxins or drugs; the latter makes them potential molecular targets for therapeutic drugs. Because of the fundamental role of K^+ currents in controlling membrane excitability, an understanding of their biophysical properties in cardiac myocytes provides a useful framework for understanding cardiac physiology. We have therefore used a method to systematically characterize the electrophysiology of the K^+ channels at room temperature. Briefly, we used cardiomyocytes from mice. We then used patch clamping to characterize the biophysics of these channels. This allowed us to get comprehensive curves of the kinetics of the K^+ channels under physiological conditions.

7.1. Introduction

VGPC are protein-complexes that allow the flux of K^+ ions in response to changes in the membrane potential and conduct approximately 100-times more readily than Na_V (Coetzee et al., 1999). The cloning and expression of the first voltage-gated K^+ channel from the *Drosophila Shaker* mutant was the starting point for investigations to identify many subfamilies, the pore, voltage sensor, gates and drug/toxin binding sites at the molecular level (Catterall et al., 2007).

VGPC include 40 different isoforms that are classified into 12 distinct subfamilies based on their amino acid sequence homology (K_v1 to K_v12) (Gutman, G. A., et al., 2003). Structurally, K_v channel α-subunits can form both tetramers of identical subunits (homotetramers), as well as heterotetramers with other proteins in the same family leading to a wide diversity of different channel complexes. Subunits of K_v1 (Shaker), K_v2 (Shab), K_v3 (Shal), K_v4 (Shaw), K_v7 (KCNQ), K_v10 (Eak), K_v11 (Erg) and K_v12 (Elk) compose functional homotetrameric channels. Subunits of other subfamilies (K_v5, K_v6, K_v8 and K_v9) usually associate with K_v2 to form functional heterotetramers.

Domains of α-subunit of mammalian voltage-gated K^+ channels can be analogous to domains of the principal α-subunit of VGCC (six transmembrane segments and one pore) (Fig. 10). The VSD (S1-S4) is sensitive to the applied voltage: depending on the direction and the magnitude of the resulting electric field, this domain accordingly changes its conformation. Within VSD, the main voltage sensor S4, is equipped with five-or-so positively charged amino acids, (arginine or lysine) at every third position. The S5–S6 segments form the pore and contain a conserved sequence (glycine-tyrosine-glycine or glycine-phenylalanine-glycine) that acts as a K^+ ion selectivity filter (SF) (Heginbotham et al., 1994). The mechanism of ion conduction at the atomic level in its selective filter has been elucidated by molecular dynamics about free energy simulations on the basis of the X-ray structure of the KcsA K^+ channel (Bernèche en Roux, 2001).

Further, the auxiliary subunits ($K_V\beta$), the main cytoplasmic protein known to interact with VGPC, modulate excitability and inactivation properties and is completely located in the intracellular side. Both the auxiliary and main subunits are located in different tissues. K_v channels expressed in the heart ($K_v1.1$, $K_v1.2$, $K_v1.4$, $K_v1.5$, $K_v2.1$, $K_v4.2$ and $K_v4.3$) vary also in their distributions and degrees of expression across the myocardium. It is this variation that is responsible for the differences in shape and duration of the atrial and ventricular APs (Rolf et al., 2000; Snyders, 1999). Some subunits of $K_v\beta1$–$K_v\beta3$ families associate with K_v1 α-subunits, while $K_v\beta4$ associates with K_v2 family members (Snyders, 1999).

The behavior of VGPC can be modified by intracellular processes, toxins or drugs; the latter makes them potential molecular targets for therapeutic drugs. Ajmaline, diltiazem, flecainide, phenytoin, propafenone, propranolol, quinidine and verapamil yield significant effects >10% on K^+ currents (Rolf et al., 2000). Tetraethylammonium (TEA) is widely used as a probe for the external mouth of VGPC. TEA binds to the permeation pathway (S5-S6) for a brief time, blocking ion flow (Pascual et al., 1995), T*yrosine or phenylalanine* in the amino acid residue in position 449 on the carboxyl terminal side of SS (Short-segments in the pore region) confers high-affinity block through cation-π orbital interactions.. However, not all cardiac isoforms are sensitive to TEA, $K_v4.2$ is relatively insensitive to TEA. $K_v1.2$ and $K_v1.5$ are resistant to TEA. $K_v2.1$ has pIC_{50} 2.0 of TEA and $K_v1.1$ requires a pK_d of 3.5 for being blocked (Attali, B., Chandy, K. G., Giese, M. H., Grissmer, S., Gutman, G. A., Jan, L. Y., Lazdunski, M., Mckinnon, D., Nerbonne, J., Pardo, L. A., Robertson, G. A., Rudy, B., Sanguinetti, M. C., Stühmer, W., Trimmer, J. S. and Wang, 2019).

Electrical properties of the K^+ currents in myocytes have been determined previously. The properties of the total K^+ current, have been recorded with the whole-cell configuration in the voltage–clamp mode (these properties depend of the electrical protocol). At 25 °C, the activation

properties, (I-V) curves fitted to a Boltzmann function, gave $V_{1/2}$ = 4.54 ± 5.87 mV, and slope k = 19.84 ± 1.72 mV. The time constant for activation (Act_τ) have been measured by fitting a single exponential curve to the recorded current trace from start of stimulus to peak current. For voltages from −10 to +80 mV, the value of Act_τ decrease from 4.68 ± 1.76 to 0.71 ± 0.15 ms. The median activation voltage (Act_Volt)—defined as the voltage where the channel current exceeds 10% of the peak current— is −31.0 mV. As for the inactivation properties, $V_{1/2}$ value of –35.26 ± 4.0 mV and k = 5.62 ± 2.01 mV from (I-V). For voltages from −20 mV to +70 mV, $Inact_\tau$ from the peak to the end of the first pulse decreased from 313.25 ± 81.7 ms to 166 ± 48.38 ms. At +70 mV, this channel inactivates as much as 57.4 ± 10%. However, it is important to consider that K^+ channels have kinetic heterogeneity and their mechanisms behind it have not been elucidated and requires further investigations (Ranjan et al., 2019). In the present chapter, we present a protocol about how to implement the whole-cell patch-clamp technique to characterize the kinetics of K^+ currents in ventricular cells.

7.2. Characterization of voltage-gated K^+ channels by the patch-clamp technique

Based on Chapter 6 - 6.2 Implementation of patch-clamp technique to the study of Ca^{2+} currents, the methodology implemented was carried out. Only differences on making patch-clamp recordings for K^+ channels are mentioned in this Chapter.

Recording solutions

For K^+ current measurements, the following solutions were used: pipette solution (in mM): KCl 140, $MgCl_2$ 2, EGTA 5, HEPES 10 and MgATP 4, adjusted to pH 7.2 with KOH, and the external bath solution (in mM): NaCl 135, KCl 5,4, $MgCl_2$ 1, Glucose 10, HEPES 10, NaH_2PO_4 0.33, with adjusted pH 7.2. To eliminate Ca^{2+} currents, Ca^{2+} channel blocker such as Cd^{2+} was used. To achieve a more complete blockade of Na^+ the external solution was supplemented with Tetrodotoxin (TTX, a Na^+ channel blocker).

Patch-clamp recordings

Recordings in whole-cell configuration, voltage-clamp mode ● TIMING 1–5 min (Chapter 2; Patch-clamp technique: voltage-clamp mode): After establishing the whole-cell recording configuration, the following recordings were made:

RECORDINGS A: Studying kinetics of activation K^+ currents:

i. For activation of total K^+ current, pulses (100 ms) were applied from a holding potential of −30 mV from −30 to + 80 mV in 10 mV steps (K_v protocol). Representative stimulation protocol traces are shown in Fig. 15.

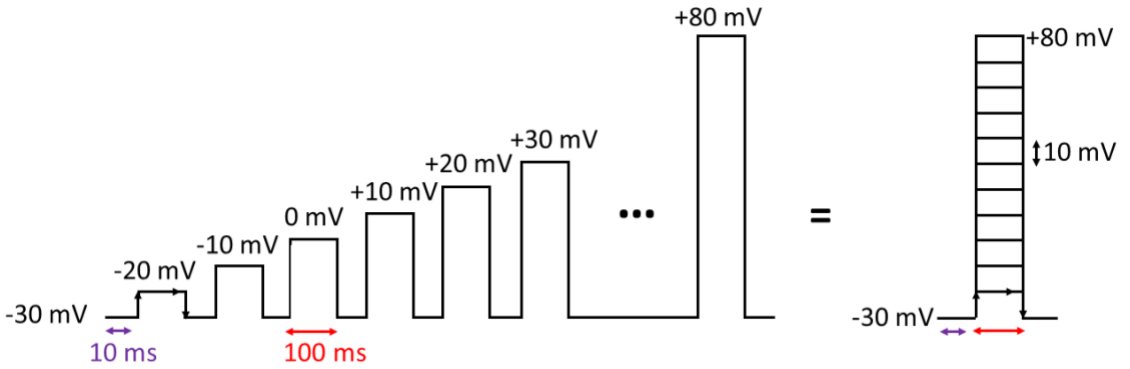

Fig. 125. Patch-clamp protocol to stimulate VGPC in myocytes. On the left the expanded protocol is shown and on the right the superposition of the pulses is shown as is typical of seeing them in research articles.

To examine effects of TEA on gating modification of K^+ currents, K_v protocol was applied without the presence of TEA in the bath solution (control current) and after treatment with TEA 100 µM. Thus, the current was plotted in terms of the time like Fig. 7a.

Chapter 8

The role of peptides from the venom gland of the spider *Pamphobeteus verdolaga* on voltage-gated calcium and potassium channels

Voltage-gated Ca^{2+} and K^+ channels are the molecular targets for a broad range of potent toxins. These peptide toxins are widely found in the venoms of arachnids. Here, we investigated the effects of six peptides isolated from the venom of the spider *Pamphobeteus verdolaga* (we named them: *vrdg66, vrdg69, vrdg164, vrdg172, vrdg177, vrdg183*) on Ca_v and K_v currents in cardiomyocytes implementing the patch-clamp technique. Our results suggest that some peptides reduced both the amplitude of Ca^{2+} and K^+ currents, other have exquisite selectivity for Ca^{2+} channels (*vrdg183*) over K^+ currents and *vrdg164* caused a shift in the voltage-dependence of activation of Ca^{2+} channels.

8.1. Introduction

A wide variety of organisms in nature contain toxins, including animals, bacteria, fungi, and plants. Many of these substances are peptides. Several strategies have been followed to identify candidates for drug development, to find a toxin capable of attacking some cell of interest, say a cancer cell or microbes, and then to direct the toxin specifically to that target (Catterall et al., 2007).

Antimicrobial peptides (AMPs) are small molecular weight proteins that are classified depending on their structure and amino acid motifs (linear α-helical amphipathic conformation, β-sheet, extended). There are three main characteristics that distinguish them: their size is between 12 and 50 amino acids; the vast majority have a net positive charge and they are generally capable of adopting amphipathic structures when they are in solution in a nonpolar medium. The best-known examples of α-helix peptides are protegrin, magainin, cyclic indolicin, and coiled indolicin. These peptides possessing an overall positive charge (in general, +2 to +9) and a large percentage (≥30%) of hydrophobic amino acid. Their amphipathicity confers the bactericidal activity and cytotoxicity (Zhang et al., 2016). Although most of them are positively charged, a few cases of negatively charged or hydrophobic helical peptides are known whose specificity is

low. β-sheet peptides are composed of at least two β-strands, cysteines with disulfide bonds between these strands (Bahar en Ren, 2013). They are generally peptides such as defensins, tachypiplesins, protegrins and lactoferricins (Fig. 16). Extended AMPs do not fold into regular secondary structure. These peptides contain high proportions of amino acids, such as Arginine, Trypsin or Proline residues.

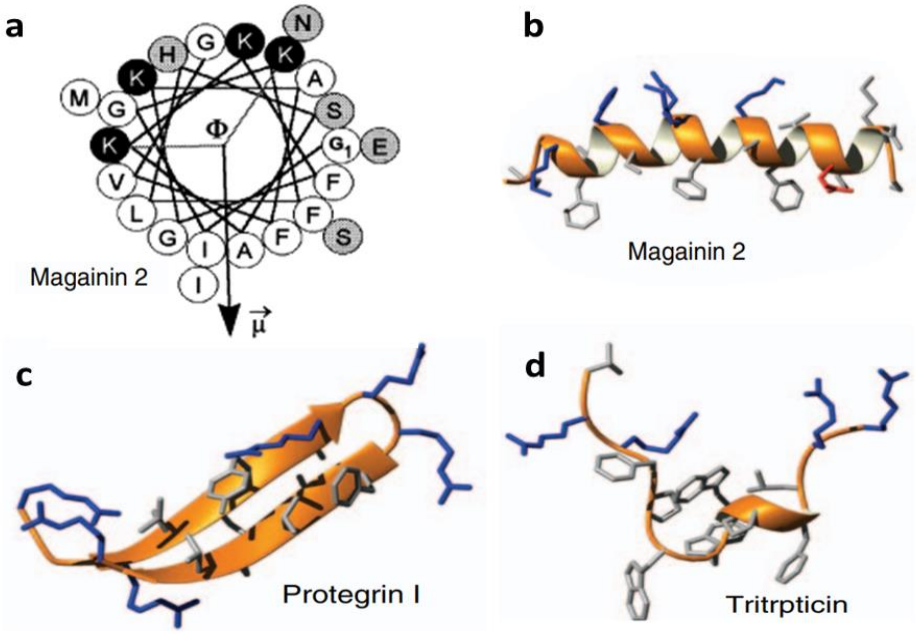

Fig. 136. Structural diversity of antimicrobial peptides. **a** Schematic drawing of the amphipathic helices of Magainin model peptide illustrating the structural features. The one letter code for amino acids is used. Hydrophobic residues are shown in white, polar residues in gray and cationic residues in black circles. The angle subtended by the charged residues on the helix surface is denoted by Φ. μ is the hydrophobic moment (Dathe en Wieprecht, 1999); **b** Side view of the Magainin peptide; **c** β-sheet peptide and **d** Extended peptide. Positively charged side chains in blue, negatively charged side chains in red and remaining side chains in grey (Nguyen et al., 2011).

AMPs exert their effect by a two-step mechanism consisting of (i) membrane permeabilization and (ii) binding to the cell surface. Membrane permeabilization causes leakage of cell contents, resulting finally in cell death. Due to most of the antimicrobial peptides are cationic, this feature ensures the initial electrostatic interaction (ionic and hydrophobic) with anionic phospholipids providing an explanation for their specificity for bacterial membranes and not for the zwitterionic lipids of the extracellular layer of eukaryotic cells (Bahar en Ren, 2013; Nguyen et al., 2011). Some mechanisms by which the peptide disrupting the integrity of the bacterial cytoplasmic membrane are shown in Fig. 17. In addition, other mechanisms explain the cytotoxic action of these toxins, include their stimulation of autolytic enzymes, transport of nutrients, respiration, proton motive force, ATP generation, intercellular communication, interference with DNA and/or protein synthesis or their binding to DNA (Bahar en Ren, 2013). Peptide toxins also block, open, and shift the gating of ion channels. Of the 274-toxin mechanisms

studied so far, 77% study ion channel–targeting toxins. From these studies, 55% were toxins selective for Na_V channels, 15% for K^+ channels, and 16% for Ca^{2+} channels (Sack, 2017).

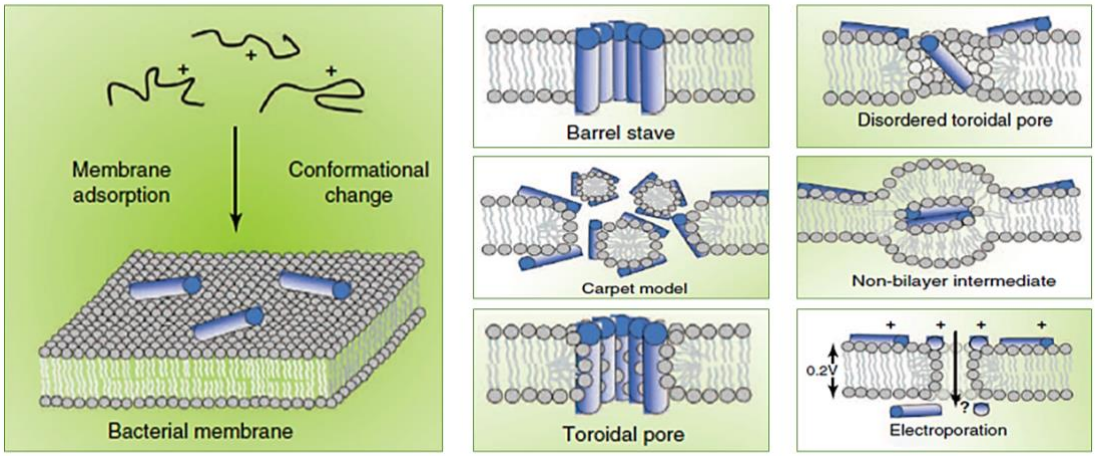

Fig. 147. Schematic representation of some action mechanisms of membrane-active AMPs. Peptides reach a threshold concentration and insert perpendicularly through the membrane to form peptide-coated pores in the barrel-stave pattern, solubilize the membrane in micellar structures in the carpet model, AMPs are always in contact with phospholipid head groups of the membrane in the toroidal pore model. In the revised disordered toroidal pore model, pore formation is more stochastic and involves fewer peptides. Non-bilayer intermediates can be induced; peptide adsorption to the membrane can be enhanced by targeting them to oxidized phospholipids; in the molecular electroporation model, the accumulation of peptide on the outer leaflet renders the membrane transiently permeable to various molecules including the peptides themselves (Deuis et al., 2017).

Peptide neurotoxins are particularly well represented in the venoms of arachnids, cnidarians and mollusks. Tarantulas are a group of often hairy and large arachnids that comprise more than 860 species. Like other venomous animals, these spiders have complex venoms dominated by disulfide-rich peptides, many of which act at ion channels to rapidly immobilize prey or deter predators. These venom peptides possess high affinity and specificity for particular classes of ion channels (King et al., 2008b) and typically bind to the less conserved VSD. All gating modifier spider peptides contain a common structural motif known as ‘‘inhibitor cystine knot (ICK)’’. As a consequence of such folding, all these peptides display a ‘‘hydrophobic patch’’ surrounded by a unique ‘‘charge belt’’ in their interaction surface (Huang et al., 2007).

Due to the percent mentioned above, the diversity of toxin action on ionic channels (voltage-dependent activation, conductance and inactivation) is usually illustrated by sodium channels, which are the molecular targets for toxins that act at least in seven allosterically coupled neurotoxin binding sites referred to as neurotoxin receptor sites 1–7 (Fig. 18a) (Catterall et al., 2007b; Huang et al., 2007; King et al., 2008c). The classic blocker TTX binds in the outer mouth of the SF and blocks the pore (Liu et al., 2019). Tyrosine helps TTX bind to Nav1.7 through a π-π stacking interaction, which is missing in $Na_V1.5$ (Figure 18b). The lack of this key interaction reduces the binding affinity of $Na_V1.5$ for TTX by up to 500-fold. Therefore, tyrosine 362 position differentiates the TTX-r channels with a Cysteine or Serine from the TTX-s with a *tyrosine or*

phenylalanine (Fig. 18c). In previous work, μ-TRTX-Pn3a, a peptide isolated from venom of the South American tarantula *Pamphobeteus nigricolor*, showed that it has exquisite selectivity for $Na_V1.7$. In contrast to TTX, Pn3a interacts with the S3-S4 linkers in DII and DIV domains (Deuis et al., 2017). Thus, it seems likely that TEA ions in K^+ channels and TTX in Na_v channels occupy similar receptor regions at the extracellular mouth of the pore when they block the channels (William, 2009).

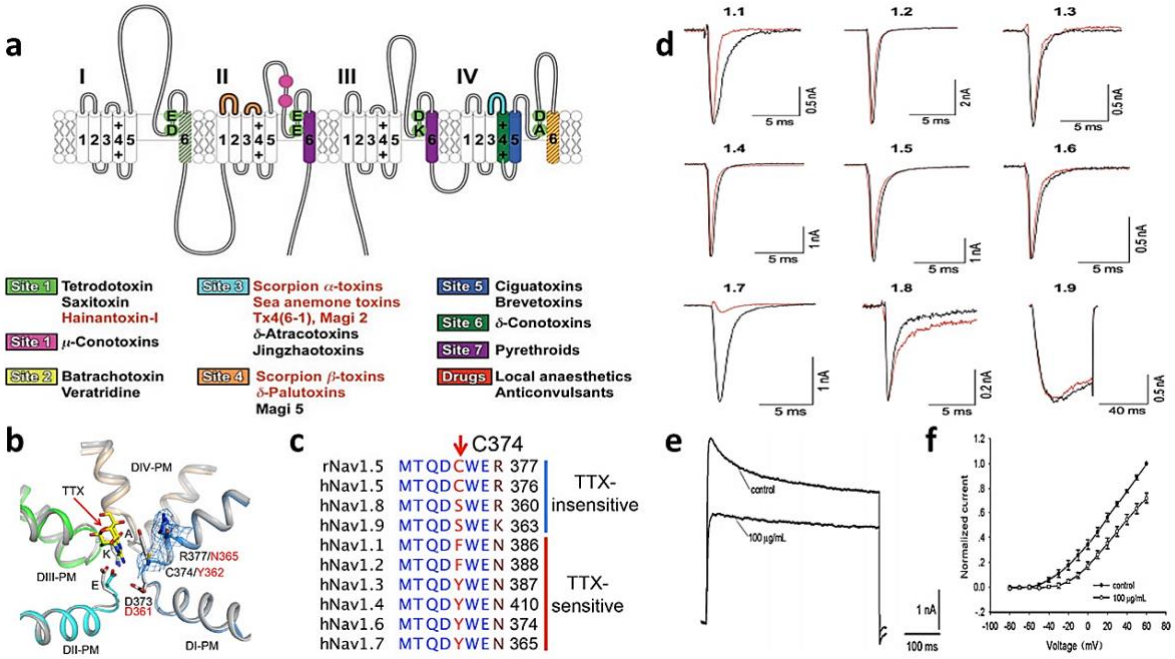

Fig. 15. Location of known neurotoxin receptor sites on Na_V channels. **a** Green circles represent the outer (EEDD) and inner (DEKA) rings of amino acid residues that form the ion SF; **b** The SF of the TTX-r $rNa_V1.5c$ (colored) versus the SF of hTTXs $Na_V1.7$ (gray) with TTX bound in yellow; **c** Sequence alignment in the region of the TTX binding site. DEKA: Asp373-Glu901-Lys1421-Ala1713; **d** Potency of Pn3a at hNaV1.1-1.9 assessed by whole-cell patch-clamp experiments. Pn3a most potently inhibited $Na_V1.7$, with 40-fold selectivity over $hNa_V1.1$, 100-fold selectivity over $hNa_V1.2$, 1.3, 1.4 and 1.6, and 900-fold selectivity over $Na_V1.5$, $Na_V1.8$, and $Na_V1.9$. Current traces before (black) and after addition of Pn3a (red); **e** Application of 100 μg/mL of venom led to a reduction of K+ currents of 44.2% ± 5.3% (n = 5); **f** Normalized current-voltage relation of K+ currents before (filled circles) and after (open circles) venom treatment, indicating that the venom altered the initial activation voltage of K+ currents (Hu et al., 2014).

Among the identified gating modifier peptides of K^+ channels, the venom of the spider *Selenocosmia jiafu* contains neurotoxins acting on VGPC in rat neurons. Patch-clamp analyses indicated that 100 μg/mL venom inhibited K^+ currents (Hu et al., 2014). Other toxins (heteropodatoxins) from the venom of a spider, *Heteropoda venatoria* have been studied. The effects of toxins on cardiac K_v1 currents were studied using patch-clamp experiments. The toxins on cardiomyocytes, blocked the transient outward K_v1 current but not other K^+ currents. These toxins slowed the time course of current activation and inactivation and shifted the voltage dependence of current inactivation to more positive potentials. The heteropodatoxins represent new pharmacologic probes to study the role of K^+ channels in cardiac and neural tissue (Blanc et al., 1998).

Diverse animal species evolved a broad range of toxic compound that have been implicated for acting on VGCC. Whole-cell patch-clamp measurements with PnTx3-6, a neurotoxin purified from the venom of the spider *Phoneutria nigriventer* on VGCC in HEK cells, indicated that PnTx3-6 inhibited L, N, P/Q and R type channels with varying potency (IC50 values of 122, 136, 263, and 607 nM respectively) (Vieira et al., 2005). Several peptide toxins acting on voltage-sensitive Ca^{2+} channels have been isolated from spider venom (Escoubas et al., 2000). ω-agatoxins block P/Q-type channels in a voltage dependent manner and modify its gating properties. ω-atracotoxins from Hadronyche species, toxins from Hololena curta, and Plectreurys toxin II, modulate insect VGCC and are useful to develop insecticides (Pringos et al., 2011). In GH3 cells, Tx3-1 was shown to increase the frequency of Ca^{2+} oscillations, while Tx3-2 partially blocks L-type Ca^{2+} channels. Other investigation of the properties of *Ornithoctonus huwena* (O.huwena), revelaed that this toxin affects the electrophysiological stability of neonatal rat ventricular myocytes by inhibiting sodium, K^+ and Ca^{2+} currents. 100 mg/mL venom inhibited 72.3 ± 3.6% I_{Na} current, 54 ± 6.1% the end current of I_{Kr}, and 65 ± 3.3% I_{CaL} current (Yan et al., 2018). Thus, toxins from spiders when act on cardiac channels, represent a multifaceted pharmacological profile because they might be valuable tools for investigation of both channels and anti-arrhythmic therapy development.

In 2016, a detailed taxonomic study allowed to recognize and to describe *Pamphobeteus verdolaga* as a new specie from the Colombian Andes, Medellín, Antioquia (Cifuentes et al., 2016; Estrada-Gomez et al., 2013). Lately, venomic, transcriptomic, and bioactivity analyses of *P. verdolaga* venom was associated with complex disulfide-rich peptides that modulate the activity on voltage-gated Ca^{2+} channels (VGCC; $Ca_v2.2$, $Ca_v3.2$), and VGSC ($Na_v1.7$) (Estrada-Gomez et al., 2013). However, the study of the effects of these peptides from *P. verdolaga* on VGIC using patch-clamp technique have never been done. In addition, the interactions of these peptides with the lipid bilayers must be investigated.

This Chapter was focused on studying the effect of six toxins synthesized from the spider *P. verdolaga* on VGCC and VGPC by implementing the patch-clamp technique. In summary, this Chapter *suggests* that these peptides could be selectively targeted to specific receptor or voltage activated Ca^{2+}, and K^+ channels. The use of patch-clamp and molecular biology techniques made possible to characterize the biophysical properties of these toxins in single cardiomyocytes and it could be a great source of biomolecules with potential therapeutic use even applications in agriculture.

8.2. Modulatory features of six novel tarantula peptides isolated from the venom gland of the spider *Pamphobeteus verdolaga* on voltage-gated Ca^{2+} and K^+ channels

Spider venom peptides from Pamphobeteus verdolaga

The Biophysics (Institute of Physics), PHYSIS (Faculty of Medicine) and Ophidism (Faculty of Chemical and Food Sciences) Groups of the University of Antioquia, joined forces to investigate the ability of peptides from the gland of *P. verdolaga* to inhibit and control the growth of resistant microorganisms and, in this way, propose the development of new biomolecules with therapeutic potential. Peptides from *P. verdolaga* were provided by the Ophidism group of University of Antioquia.

Six peptides (*vrdg66, vrdg69, vrdg164, vrdg172, vrdg177, vrdg183*) were chosen to evaluate their effect on K^+ and Ca^{2+} currents because they have cysteines with disulfide bonds between their strands (Fig. 19). Furthermore, due to their amino acid sequence and the results of the growth inhibition percentage (data not shown), it was considered that these peptides were the best candidates to carry out their biophysical characterization using the patch-clamp technique. Synthetic peptides from *P. verdolaga* were kindly provided by the Ophidism group of University of Antioquia and were used for all further experiments.

Toxin name	Molecular weight (g/mol)	Hydrophobic moment	Charge	Isoelectric point	Solubility (mg/ml)
vrdg66	1124,44	0,37	5	11,15	> 8
vrdg69	1146,4	0,06	2	8,7	2
vrdg164	1811,22	0,07	5	10,8	2
vrdg172	2148,63	0,06	5	9,8	4
vrdg177	2276,76	0,06	5	9,8	4
vrdg183	2233,82	0,06	5	9,8	4

Fig 19. Photo of the *Pamphobeteus verdolaga* specimen from which venom was obtained with the electrical properties of six synthesized peptides selected for this study (Cifuentes et al., 2016). The lyophilized toxins were provided by the Ophidism group of University of Antioquia. Scale bar: 10 mm.

Electrophysiology

Synthetic peptides were dissolved in deionized water, divided into aliquots and stored at -80 °C. On the day of experiments, individual aliquots of *vrdg* were thawed on ice, and carefully added to the bath solution (10^{-4} M).

For evaluating ionic current gating modification by the six *P. verdolaga* peptides the **Recordings A and B in whole-cell configuration, voltage-clamp mode** (*Chapters 4 and 5*) were made both under control conditions and after putting the peptides in contact with the extracellular solution.

All *vrdg* effects were compared to pre-toxin control parameters within the same cell**.** Chamber must be thoroughly cleaned after each experiment.

To evaluate if the effects of *P. verdolaga* peptides are reversible and dose-dependent, Ca^{2+} and K^{+} currents will be obtained during depolarizations to 0mV without toxin (control) and after treatment with different doses of peptide in the bath solution. After modification with *P. verdolaga* peptides, it is possible to determinate changes on voltage-dependence for activation, positive and negative shifts in activation and inactivation voltages, slow and fast inactivation, steady-state fast or slow activation with midpoints, among others. Furthermore, for some peptide toxins, modification of activation of channels is strongly facilitated by a brief depolarizing pre-pulse applied before to the main protocol, for that reason, a pulse of 50 mV for 2 ms can be applied before to Ca_v and K_v protocols when peptides are used. All experiments were recorded before and after application of *P. verdolaga* peptides and thus each cell serve as its own control.

Chapter 9
Results

9.1. Our Langendorff apparatus makes successful isolation of cardiomyocytes from the adult mouse heart

Cannulation and retrograde perfusion of the aorta, is widely adopted for myocyte isolation from the adult mouse heart. Thus, the methodology outlined in Fig. 9 was implemented. For each experiment, enzymatic tissue digestion was monitored, and total cell number and percentage of viable rod-shaped myocytes were subsequently inspected under the inverted microscope (20× objective lens). CM remained adhered to the recoding chamber displaying characteristic morphology and clearly organized sarcomeric striation patterns (Fig 20).

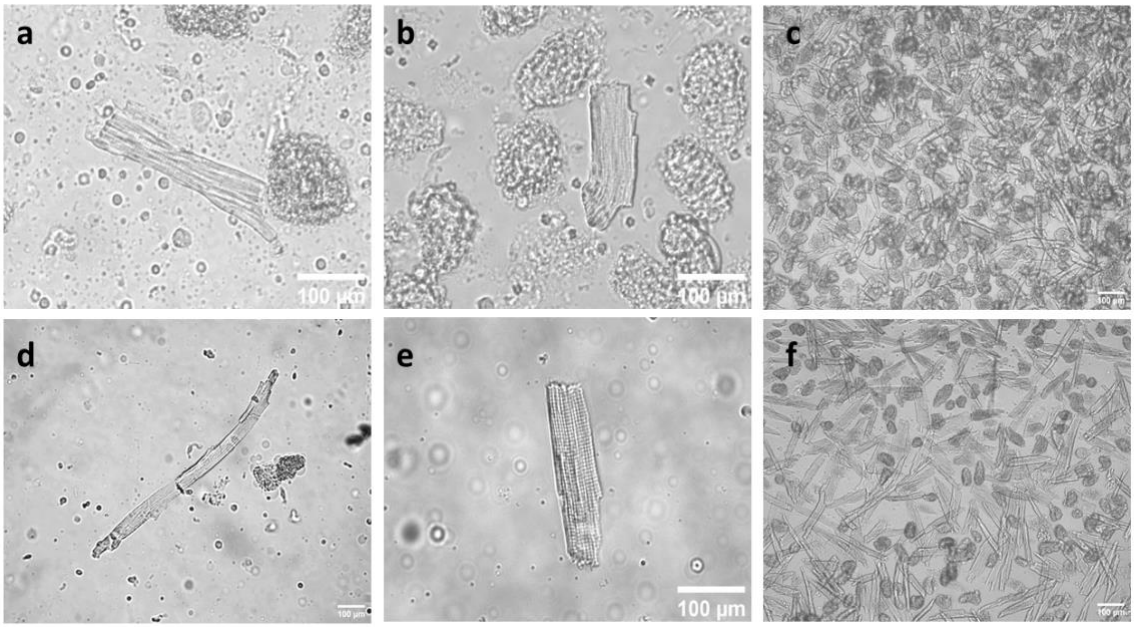

Fig. 20 Representative images of adult mouse ventricular digestion products, before (**a,b,c**) and after improvements (**d, e , f**). **a** CM obtained without filtering solutions with nitrocellulose filters; **b-c** Containing many rounded and hypercontracted cells. Rounded cells were considered to have been irreversibly injured or dead; **d** Ventricular myocytes firmly adhered to each other; **e** Showing a viable single myocyte, with organized sarcomeric striations, rod-shaped morphology and sharp-edged membrane. **f** Image showing a majority of healthy cells, highest viable yields were obtained at dissociation buffer with pH 8. Loss of sarcomeric organization was observed after 6-hours. Scale bars =100 µm.

Optimal morphology of cells was most reliably achieved at dissociation buffer pH 8 (Figs. 20e and f, and Fig. 21a). With these conditions, the protocol reproducibly yields hundreds of myocytes viable, with cylindrical-shaped cells. Furthermore, the protocol was found to be compatible with

automated infusion pumps for controlled delivery of used digestion buffers (Fig. 21c). Flow rates of 4,5 mL/min produced average yields of over 60% rod-shaped cells, demonstrating success in the methodology.

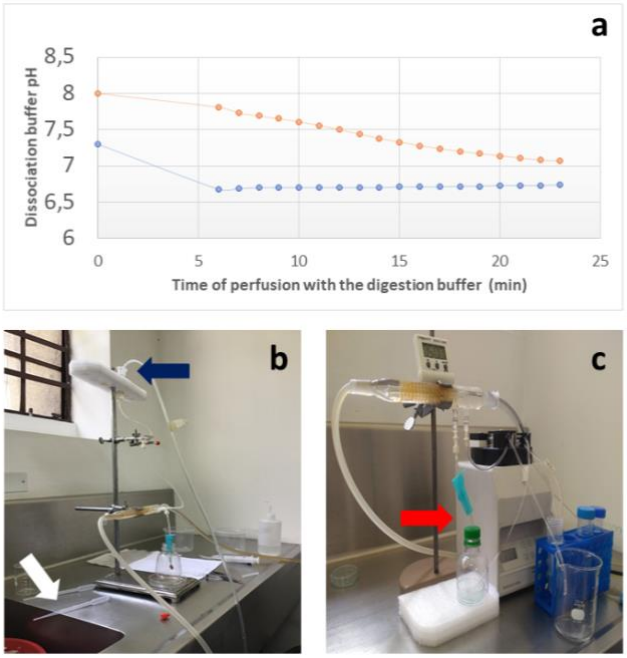

Fig. 21. Some improvements in our simplified setup for isolating viable cardiac myocytes. **a** Enzymes drastically decrease the pH of the buffer solutions. Buffer starts with pH 8 in orange, with pH 7.3 in blue. **b** Manual system of retrograde perfusion (before). Here the solutions were recycled to the reservoir by Pasteur pipettes from the white arrow to the blue; **c** Modified and simplified Langendorff system whit a peristaltic pump incorporated (after)**.**

The digestion degree of the heart affects the results of viable cells. Either insufficient or excessive digestion will decrease the success rate of the experiments. The digestion time of heart was mainly determined by the mice weigh. Therefore, Table 3 provides a simple and effective approach to judge the degree of digestion.

Table 3. Time of enzymatic digestion depending of the mice weigh.

Swiss Webster mice weigh (g)	Time of perfusion with the digestion buffer (min)
20-21	18
22-23	19
24-26	20

9.2. Isolated cardiomyocytes display normal cardiac currents

To confirm the amenability of isolated CMs to patch-clamp studies, cardiac currents were quantified in freshly isolated ventricular myocytes (Fig. 22). The membrane capacitance was 138.64 ± 25.12 pF/cell (n=100). Measurements of whole cell under voltage-clamp mode were evoked in all cells tested. The current amplitude analysis was conducted on the traces obtained with the step protocols. The peak I_K current density measured was 18.1 ± 1.7 pA/pF (n=5). The amplitude of the unitary currents depended on the holding potential and was reduced when the recording pipette contained 150 µM TEA (n=3). The blocking rate was significantly voltage-

dependent. I_K displayed robust voltage dependence with a mean $V_{0.5}$ of −30 ± 1 mV and reverse potential of -83 ± 2 mV. We obtained current-voltage (I–V) relationships by plotting the amplitude of the steady-state component of these currents against the membrane potential. For Ca^{2+} channels, the peak current-voltage relation revealed a threshold at about -30 mV and a reversal potential close to 50 mV. The maximum amplitude was near 0 mV. The whole-cell I_{Ca} also was characterized by pharmacological tools. I_{Ca} was completely blocked by 13 µM nifedipine (n=4). These values are consistent with previous reports of ventricular cardiac currents measured under similar conditions (Maltsev et al., 1994). Thus, the currents were measurably preserved using our isolation technique.

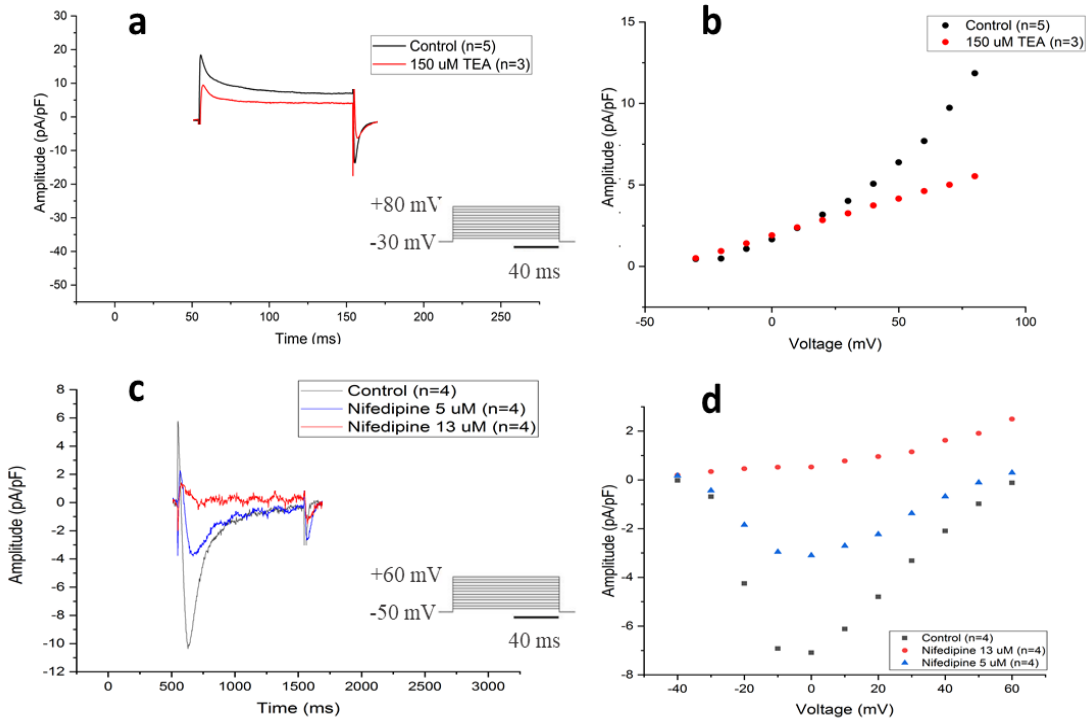

Fig. 22. Representative cardiac experiment recorded from a single ventricular myocyte using patch-clamp. **a** Characterization of outwardly K^+ currents in cardiomyocytes. Currents were evoked by 100 ms voltage-steps from −30 to +80 mV in 10 mV increments from a holding potential of −30 mV; TEA (150 µM) partially blocks the transient outward current. I_K current density (pA/pF; n=5 cells); **b** Current-voltage (I-V) relationship; **c** Graph showing electrophysiological characterization of the Ca^{2+} inward current; **d** Superimposed I_{Ca} current traces correspond to the I-V relation. Current in absence of Nifedipine (▪). The voltage protocols are shown in the inset. Toxin and drug exposure time was 8 ± 1 min.

9.3. The role of peptides from the venom gland of the spider *Pamphobeteus verdolaga* on voltage-gated Ca^{2+} and K^+ channels

Electrophysiological Studies

The effect of *vrdg* peptides on channel activation was studied using isolated cardiomyocytes. Figs. 23 to 28 show normalized K^+ and Ca^{2+} currents without (Pre) and with these peptides (Pos). We

examined the effect of *vrdg* peptides on the current-voltage (I-V) relationship as well as the voltage-dependence of activation. Detailed channel selectivity characterization using whole-cell electrophysiology revealed that *vrdg69* (1 µM) simultaneously inhibited VGPC (reduction of 52,5% I_K peak, Figs. 23a and b) and VGCC (reduction of 63,3% I_{Ca} max, Figs. 23c and d). Isoproterenol (ISO) (10^{-5} M) rapidly increased I_{Ca} 32,8% (Figs. 24e and f). The I_{Ca} started to rise usually within 10 min after application of ISO, and the response reached maximum within 15 min. After ISO *vrdg177* (1 µM) was added to the bath solution (Figs. 24e and f). The amplitude of I_{Ca} was inhibited 57,1% of I_{Ca} peak. Similar results were obtained with *vrdg177* because had reduction of 59,1% I_K peak (Figs. 24a and b) and 61,8% for I_{Ca} peak (Figs. 24c and d).

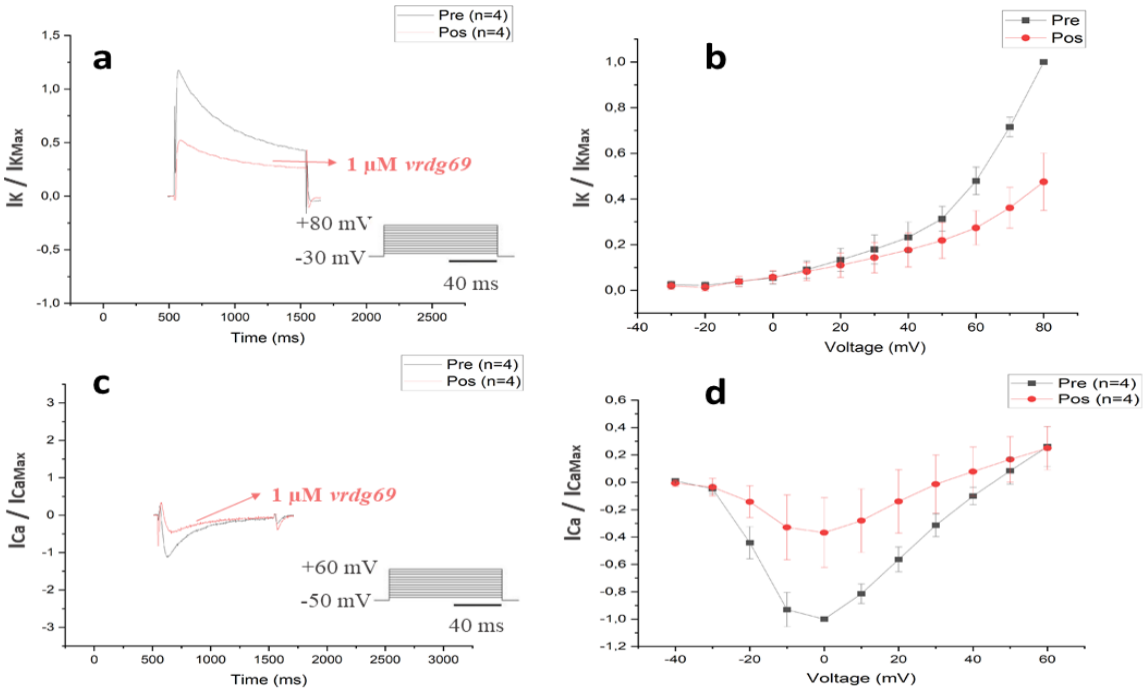

Fig. 23. Voltage-dependent inhibition by *vrdg69* of VGPC and VGCC expressed in ventricular myocytes. **a-b** I-T and I-V curves before (black line and squares) and after addition of *vrdg69* (red line and circles), *vrdg69* (1 µM) inhibited K^+ currents and **c-d** Ca^{2+} currents (n=3). The voltage protocols are shown in the inset. Currents without (Pre) and with toxins (Pos). Currents from each cell were normalized to their maximum amplitude.

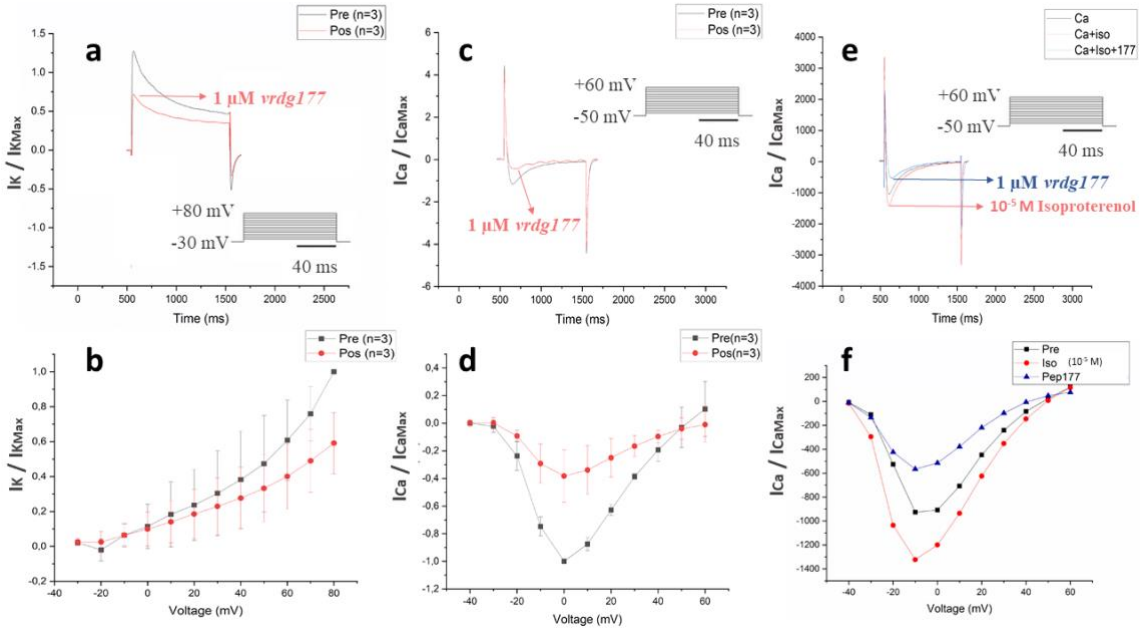

Fig. 24. Voltage-dependent inhibition by *vrdg177* of VGPC and VGCC expressed in ventricular myocytes **a-b** I-T and I-V curves before (black line and squares) and after addition of *vrdg177* (red line and circles), *vrdg177* (1 µM) inhibited K^+ currents and **c-d** Ca^{2+} currents (n=3); **e-f** Superimposed I_{Ca} traces evoked by various depolarizing steps (-50 to + 60 mV) in the absence (control) and presence of ISO (10^{-5}M) and *vrdg177* (1 µM). **Ca**: Control, **Ca + Iso**: Bath solution with 10^{-5} M of ISO, **Ca + Iso + 177**: Bath solution with 10^{-5} M of ISO and 1 µM of *vrdg177*. The voltage protocols are shown in the inset. Currents without (Pre) and with toxins (Pos). Currents from each cell were normalized to their maximum amplitude.

On the other hand, *vrdg66* (1 µM) mainly inhibited VGPC (reduction of 24,4% I_K peak, Figs. 25a and b) over VGCC (reduction of 16,3% I_{Ca} max, Figs. 25c and d). Similar affinity was obtained with *vrdg172* (1 µM) with a reduction of 43,9% I_K peak (Figs. 26a and b) over 38,9% for I_{Ca} peak (Figs. 26c and d).

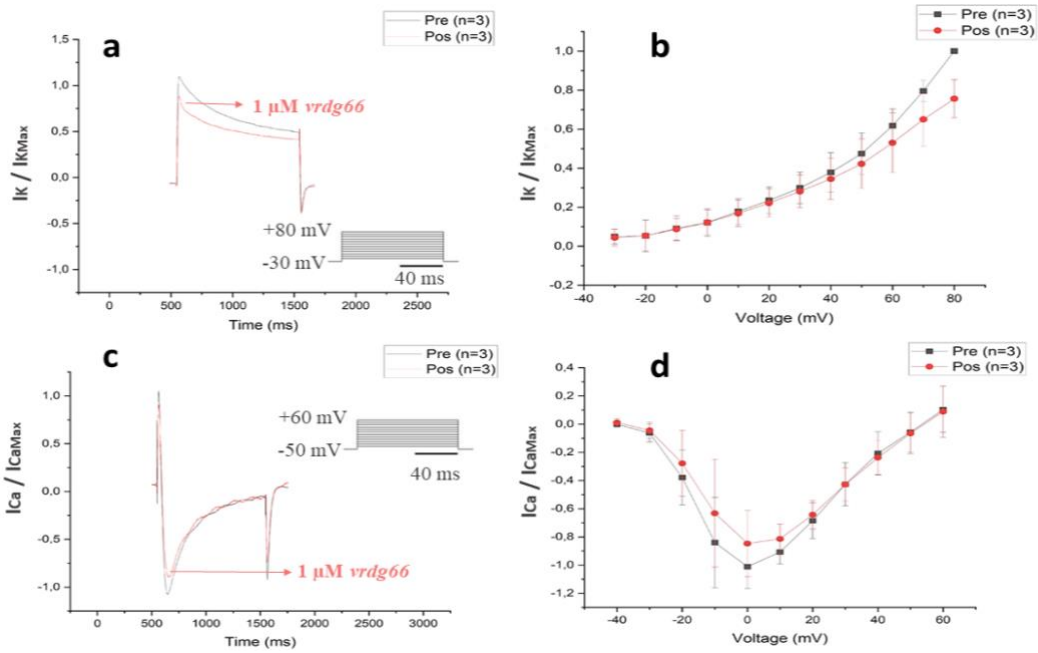

Fig. 25. Voltage-dependent inhibition by *vrdg66* of VGPC and VGCC expressed in ventricular myocytes. **a-d** I-T and I-V curves before (black line and squares) and after addition of *vrdg66* (red line and circles), *vrdg66* (1 µM) mainly inhibited K^+ currents over Ca^{2+} currents (n=3). The voltage protocols are shown in the inset. Currents without (Pre) and with toxins (Pos). Currents from each cell were normalized to their maximum amplitude.

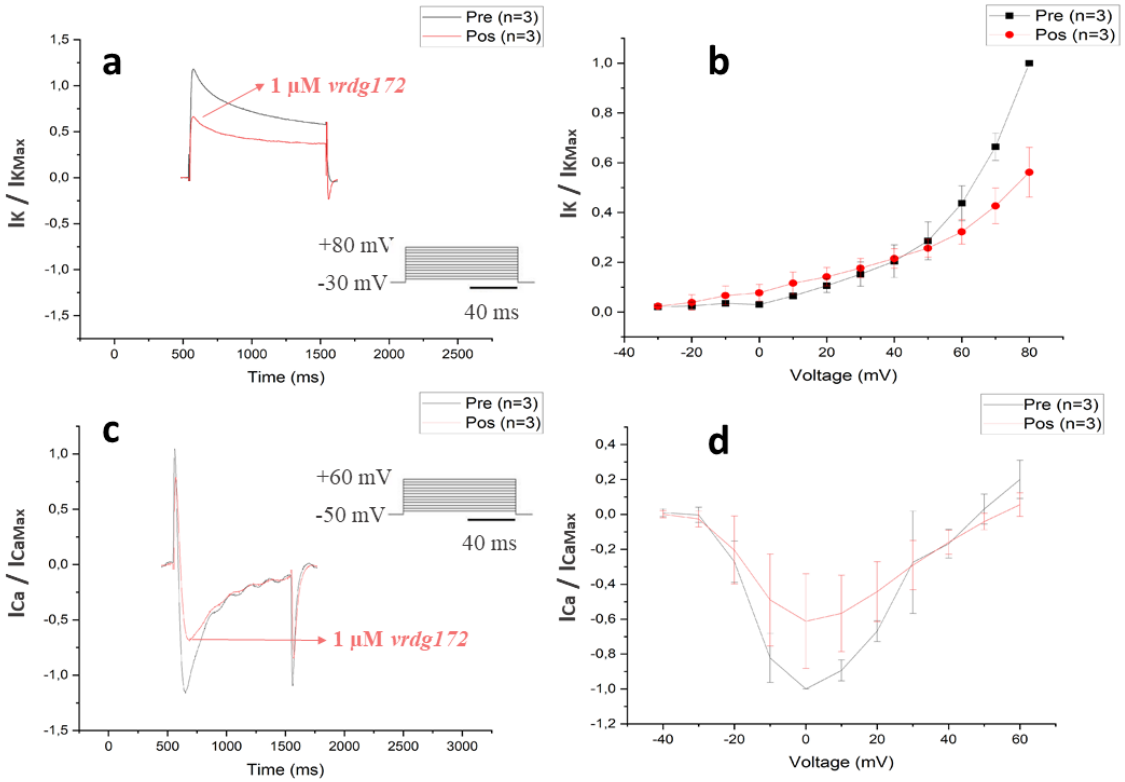

Fig. 26. Voltage-dependent inhibition by *vrdg172* of VGPC and VGCC expressed in ventricular myocytes. **a-d** I-T and I-V curves before (black line) and after addition of *vrdg172* (red line), *vrdg172* (1 µM) mainly inhibited K^+ currents over Ca^{2+} currents (n=3). The voltage protocols are shown in the inset. Currents without (Pre) and with toxins (Pos). Currents from each cell were normalized to their maximum amplitude.

At a concentration that abolished inward current at Ca^{2+} channels (66.7% reduction in maximum amplitude, Figs. 27c and d), *vrdg183* (1 µM) had little effect on the current traces for K^+ channels (6.2% inhibition of I_K peak, Figs. 27a and b). This result shows that *vrdg183* was one of the most selective *vrdg* inhibitors.

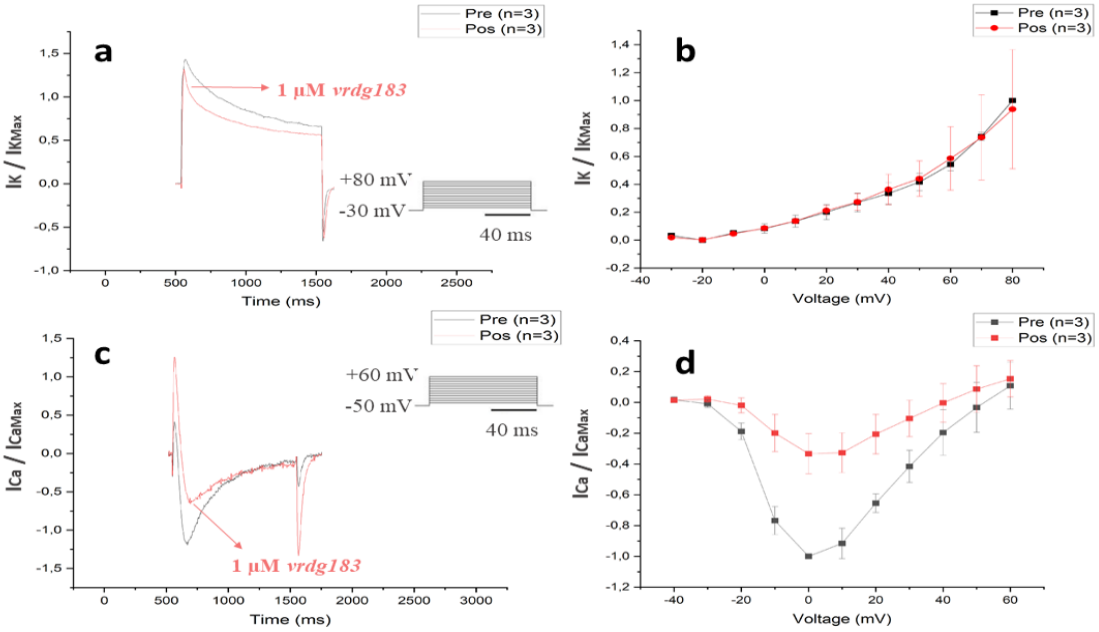

Fig. 27. Voltage-dependent inhibition of VGPC and VGCC by *vrdg183* (n=3). **a-d** I-T and I-V traces recorded in the absence (black line) and presence of *vrdg183* (red line), *vrdg183* (1 µM) mainly inhibited Ca^{2+} currents over K^+ currents. The voltage protocols are

shown in the inset. Currents without (Pre) and with toxins (Pos). Currents from each cell were normalized to their maximum amplitude.

At VGCC, *vrdg164* (1 µM) shifted the voltage-dependence of activation to more depolarized membrane potentials, showing gating modifier activity (Fig. 28c and d). Interestingly, this effect on the voltage-dependence of activation was unique to *vrdg* toxins on Ca^{2+} channels. *Vrdg164* (1 µM) had no significant effect at K^+ channels (14,4% inhibition of I_K peak, Figs. 28a and b).

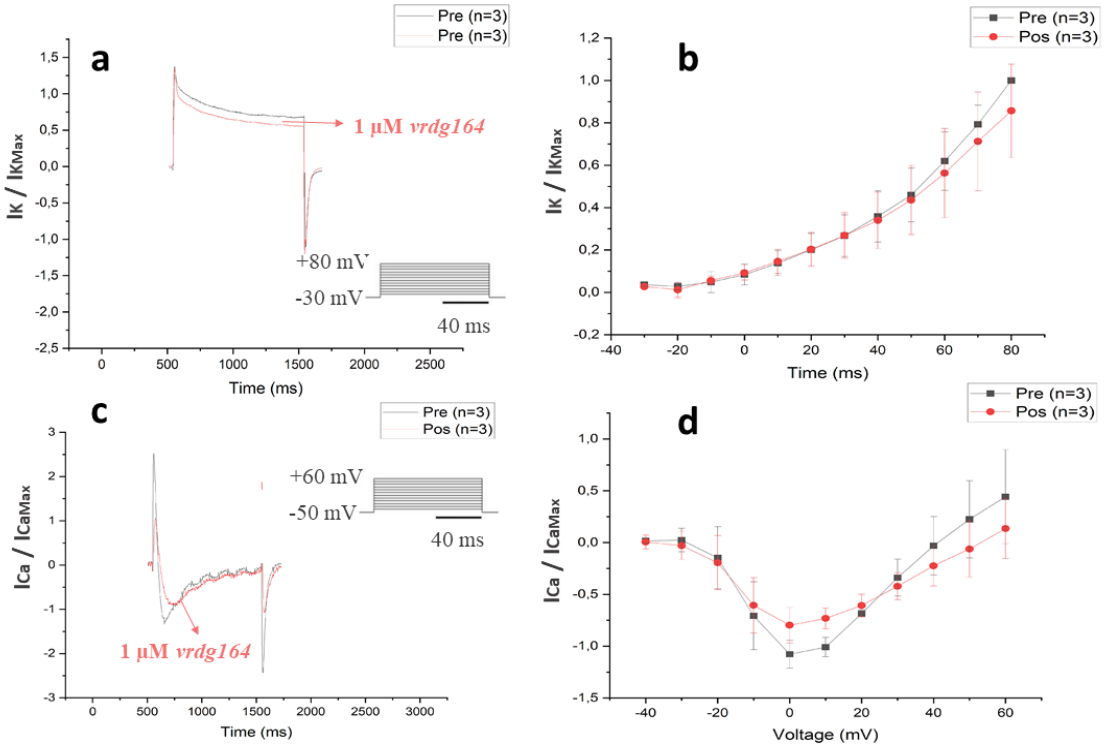

Fig. 28. Voltage-dependent effect of VGPC and VGCC by *vrdg164*. **a-d** I-T and I-V traces recorded in the absence (black line) and presence of *vrdg164* (red line), *vrdg164* (1 µM) mainly inhibited Ca^{2+} currents over K^+ currents. *vrdg164* (1 µM) caused small but significant shifts in the $V_{0.5}$ of activation at VGCC only. The voltage protocols are shown in the inset. Currents without (Pre) and with toxins (Pos). Currents from each cell were normalized to their maximum amplitude. Data were presented at mean ± SEM (n=3).

Chapter 10
Discussion

10.1. Cardiac cells

The extraction protocol of cardiomyocytes requires careful execution during cannulation of the aorta and appropriate heart perfusion, for obtaining the maximum number of functional cells. After cleaning around the aorta, place the heart with lungs for locating the heart and visualizing the perfusion of the coronary arteries. The position of the needle insertion is not inserted too deep through the aortic valve in order to help the collagenase fully interact with heart tissue during coronary circulation. If the blood does not begin to discharge after perfusion, the injection needle may be positioned incorrectly.

Selection and concentration of enzymes with collagenolytic activity, buffer solutions, temperature, pH, 95% O_2 and 5% CO_2 flow, perfusion volume, and standardizing the criteria for termination of digestion time, were fundamental for obtaining single cells that maintain their properties for a suitable period after extraction. Viable and functional cardiomyocytes with the characteristic roughly rod-shaped morphology with rectangular ends and clear cross-striations were obtained from adult mice heart through our protocol as has been reported in the literature (Balse et al., 2012; Li et al., 2014; Mitcheson et al., 1998). Enzymes drastically decrease the pH of the buffer solutions; thus, optimal morphology of cells was most reliably achieved at dissociation buffer pH 8 (Fig. 21a). With these conditions, the protocol reproducibly yields hundreds of myocytes viable. In our results, about 60% cells were isolated during each experiment. Around 3 million cardiomyocytes could be obtained from an adult rat heart (Campora et al., 2018).

We have optimized the Langendorff system for retrograde perfusion compatible with automated pump injection systems, for precise control of buffer pressure or flow rates, and provided standardized protocol for isolating adult mouse heart by establishing the cardiomyocytes with high purity and viability achieving from our methodology will facilitate the acquirement of high-quality cardiomyocytes for patch-clamp experiments, and provide gentle cell isolation that increases the yield of single cardiomyocytes suitable for biophysical researches in our laboratory.

10.2. Ca^{2+} and K^+ currents in cardiac cells

We demonstrate that some basic cardiac-specific ionic currents, I_{Ca} and I_K, are expressed in our cells. All major biophysical and pharmacological properties of these ionic currents were identical to previously descriptions (Nuss en Marban, 1994). To record calcium currents, potassium channel blockers were added to the internal and external recording solutions. Most K^+ channels are blocked by Cs ions. CsCl blockade due to cesium ion is larger than the pore size of the potassium channel, thus blocking the channel (Cecchi et al., 1987, (IUPHAR/BPS Guide to PHARMACOLOGY, 2022). Therefore, adding cesium inside the pipette blocks only outward currents. However, when conditions favor inward rectification, K^+ in external solution can still find entry, so it was necessary to add cesium in the external solution and supplement with TEA. K^+ currents were sensitivity to the pore-blocking agent TEA (by binding at aromatic residue of the channel structure) when it was applied to the extracellular side of the membrane as has been reported in the literature (Heginbotham en MacKinnon, 1992). To record potassium currents, Ca^{2+} currents and Na^+ currents, were blocked by implementing electrical protocols. Similarly, to VGPC, VGCC currents were totally blocked by nifedipine when a concentration of 13 µM was used. These data suggest that nifedipine inhibition on these channels (influenced by extracellular divalent cations) confirm the amenability of our isolated CMs to patch-clamp studies (Heginbotham en MacKinnon, 1992). If we had not used blockers, the total current would have been the sum of all cardiac currents (Eqs. 1.7 and 1.13).

Cell electric capacitance depends on the shape of the cell and the membrane thickness (Eq. 1.4) (Heginbotham en MacKinnon, 1992). Experimental data about the electric capacitance of cardiomyocytes was collected, the typical capacitance of adult mammalian ventricular myocytes is 100-200 pF (Nuss en Marban, 1994), and confirm the efficacy of the patch-clamp setup used in the present work (Platzer en Zorn-Pauly, 2020).

10.3. Characterization of the effect of six synthetic peptides on Ca^{2+} and K^+ currents

We have characterized the effect of six synthetic peptides, that are abundant in the venom of the tarantula *Pamphobeteus verdolaga* (*vrdg66, vrdg69, vrdg164, vrdg172, vrdg177, vrdg183)* using the whole-cell voltage-clamp technique. Although there are adequate recommendations for naming peptides derived from spiders (King et al., 2008c), we propose this simple nomenclature to recognize peptides for internal experiments. These toxins are modulators of both K^+ and Ca^{2+} channels. Although a variety of natural products target voltage-gated channels (Adams, 2004; Frazão et al., 2012; Lewis et al., 2012; Olivera, 1997; Possani et al., 2000) these six spider toxins are the first known agents from a new Colombian species that produce changes on the kinetic

characteristics of these ionic currents. *vrdg* peptides share striking structural and functional similarities to other ICK gating-modifier toxins and although all these peptides belong to the class of ICK peptides, they are almost completely dissimilar. Given the high potential of innovation and future patenting, it is not possible to present in detail the sequences and structures of the peptides.

vrdg66 (1 µM) has the shortest sequence and the highest percentage of bacterial growth inhibition however, it had the smallest current inhibition percentage on I_{Ca} and $I_{K,}$ mainly on VGPC. *vrdg69* did not have a significant percentage of bacterial growth inhibition but potent inhibited both I_{Ca} and I_K (1 µM). *vrdg172, vrdg177, vrdg183* only differ by one or two amino acids in their sequences. ISO increased I_{Ca} (through mechanisms that involve the pertussis-toxin-insensitive G proteins (Xiong et al., 1994)) but once *vrdg177* (1 µM) was in contact with bath solution, the peak current was reduced. This peptide had a modular effect similar to *vrdg69,* nevertheless, it has a large bacterial growth inhibition percentage and its amino acid sequence is longer. *vrdg172* had a specific effect like *vrdg66* (mainly on VGPC). Given that *vrdg66, vrdg69, vrdg172 and vrdg177* modulate both K^+ and Ca^{2+} channels it would be of interest to determine how conserved the binding domains are in these two channels.

vrdg183 (1 µM) partially inhibits Ca^{2+} channels (blockade > 65%) by decreasing peak current whereas under the same conditions, K^+ currents were not affected. *vrdg164* (1 µM) shifted the voltage-dependence of activation to more depolarized membrane potentials of Ca^{2+} channels, whereas there was not the same effect on K^+ channels. High selectivity is important, since activity at other channel and even isoforms, likely contributes to physiological activity but also adverse effects (Deuis et al., 2017). To analyze in detail if *vrdg164* and *vrdg183* are dose-dependent we are testing different dose in the same cell.

Previous patch-clamp studies have shown that peptides derived from spider venoms act either as pore blockers (PBs) (that bind to the extracellular side of the channel pore) or as gating modifiers (GMs) (that bind to the voltage-sensing domains of VGIC channels) to modify the gating associated with channel activation and inactivation. (Agwa et al., 2020; Männikkö et al., 2018; Zhang et al., 2018). Although the molecular binding site of *vrdg* peptides are unknown, our results suggest that *vrdg183* selectively could act to occlude the external pore (PBs) of the Ca^{2+} channels and *vrdg164* could be a selectively GM of VGCC.

Improved understanding of these synthetic peptides may be an important advance in the development of therapeutic agents. Our peptides could be comprised of different classes of

molecules displaying wide-ranging pharmacological activities. Most toxin-based approved drugs are derived from animal venoms. SNX-111 from the venom of the fish-hunting snail *Conus magus* blocks Ca_v channels leading to antinociception. SNX-111 is a valuable advantage in comparison to morphine. Phα1β, is classified as P/Q- and N-type voltage-gated calcium channel blocker, and demonstrated analgesic effects. PhTx3-3 (also a voltage-gated calcium channel blocker) had inhibitory effects on the proliferation and viability of different glioma cell lines. Electrophysiological studies of Phα1β on calcium currents showed significant reductions of tumor areas. K_v currents are considered potential bioactive molecules to treat autoimmune diseases. HsTX1 from Heterometrus spinifer venom reduce inflammation in the induced arthritis. ImKTX88 from Isometrus maculatus ameliorates pathological severity in autoimmune encephalomyelitis. Ktx from Androctonus mauretanicus mauretanicus venom prevent bone loss, has been implementing to treat periodontal disease and rheumatoid arthritis. MgTX from Centruroides margaritatus venom has been considered as a novel therapeutic target for lung adenocarcinoma therapy. Ts6 and Ts15 from Tityus serrulatus venom reduce inflammation. ShK-186 isolated from Stichodactyla helianthus sea anemone venom, acts as a $K_v1.3$ inhibitor reducing multiple sclerosis (Bordon et al., 2020). *P. verdolaga* venom is rich source of molecules with a wide range of applications. However, to make the use of these molecules, extensive preclinical trials are necessary.

Chapter 11
Conclusion

In conclusion, the flexible and adaptable Langendorff system was a useful tool for isolating cardiac cells. These factors support the conclusion that we have standardized a highly reproducible protocol for isolating viable cardiomyocytes murine cells from the adult mouse heart, suitable for biophysical investigations concerning to cardiac mechanisms at the cellular level. We demonstrate that all major biophysical and pharmacological properties of cardiac currents, I_{Ca} and I_K, were identical to those previously described for adult cardiomyocytes. The electrophysiological characterization of cardiomyocytes using the patch-clamp technique allowed us to ensure that our cells corresponded to the model of interest, and allow us to ensure that our results are reliable. The effects on the currents generated by the pharmacological agents used (Nifedipine and Isoproterenol) and blockers known as tetrodotoxin and tetraethylammonium, show that we had the specific calcium and potassium currents, and also that their activation signaling pathways were functional. Additionally, it demonstrates that the cells were in good viability conditions necessary for the experiments with the peptide toxins. Additionally, the electrical properties obtained during the implementation of the patch-clamp technique (cell capacitance, series resistance, seal resistance, tau, etc.) suggest that the gigaseals were of high quality and there was adequate voltage control.

We present the first characterization of effects of *Pamphobeteus verdolaga* peptides on calcium and potassium channels by the patch-clamp technique. We conclude that, *vrdg66, vrdg69, vrdg164, vrdg172, vrdg177, vrdg183* modulate Ca_v and K_v currents in cardiomyocytes. vr*dg172, vrdg66, vrdg69 and vrdg177* affect both K_V and Ca_V. The NDBP *vrdg66,* had the smallest current inhibition percentage which showed that the modulation of ion channels is poor due to the absence of disulfide bridges. *vrdg164* delayed the inactivation process of Ca^+ currents, giving a hypothesis that could be a GMs to bind to the VSD. Petide toxins like ω-Aga-IVB, ω-grammotoxin-SIA: kurtoxin, SNX-482, ProTx-1, and ProTx-2 shift calcium channel gating in the depolarized direction to unphysiologically positive voltage. In the presence of these GMs, channels activate more slowly and deactivated more quickly (McDonough, 2007). We conclude that *vrdg183* decrease the calcium current density. This peptide could be a PB binding to the extracellular side of the channel pore modifying the amplitude. v-ACTX-Ar1a, and its homolog v-ACTX-Hv1a

from Hadronyche versuta for example are PB due to block insect calcium channel currents. These findings validate PB as potential for insecticides (Chong et al., 2007).

In this way, the results of this degree work are the first to report about novel spider toxins that modulate Ca_v and K_v in mammals. Due to the potent effects of *vrdg164* and *vrdg183* had on cardiac cells, we recommend not to use them as antimicrobials. In addition, some of these spider toxins could ultimately become the defining pharmacology for certain illness, for example, Pn3a μ-theraphotoxin-Pn3a, isolated from venom of the tarantula *Pamphobeteus nigricolor*, potently inhibits voltage-gated-sodium channels ($Na_V1.7$) and this toxin is a useful pharmacological tool to inhibit the pain (Deuis et al., 2017). In addition, these new peptides could be novel molecular tools for ion channel characterization.

Reliability

Pre-currents: The one with the best electrical properties was chosen.

Pos-currents: Although the recordings can last 40 minutes, the current between 5-10 minutes after application of the peptide was chosen. After that time, there may be a run-down in the cell that would skew the results.

Strengths and weaknesses:

Cells with homogeneous geometries were chosen to ensure good voltage control.

Solutions were kept on ice while in use to reduce bacterial growth and prevent degradability (e.g. ATP).

Access resistance was low while executing an experiment by patch-clamp. The best electrical properties were always guaranteed during each experiment (e.g. Tau, gigaseal, etc.). If this is not possible, the experiment was discarded. The membrane capacitance was chosen from the current obtained with the best electrical properties.

High skills and experience was acquired to move the glass pipette over the single cell for measuring current changes across the membrane through ion channels without damaging the cell, pipette or configuration.

Patch-clamp technique offers high sensitivity (pA resolution). Noise was minimized thanks to the high technology of the electrophysiology equipment used in the laboratory.

Patch-clamp technique is especially useful in the study of excitable cells (e.g. cardiomyocytes). Isolated cells represent simplified systems whose electrophysiological responses are controlled. The external and internal side of the cells, protocols, etc., can be controlled by the experimenter.

Ions, toxins, and other pharmacological agents can be applied easily in stablished concentrations, even on the same membrane patch, facilitating generation of dose–response curves.

There are, of course, limitations to the model exercises presented here. A problem with whole cell recordings is a chance of dialysis of cell content due to the intrinsic disruption of the natural intracellular environment. Too much negative pressure to seal or break the membrane was not applied, this could injure the cell.

Patch-clamp configurations penetrate the pipette through the membrane at and could disrupt the natural cell physiology. Thus, the implementation of patch-clamp for several minutes is unsuccessful due to the decay of intracellular signals (run-down).

Patch electrodes are not reusable. It is only experimented with completely clean pipettes, once the experiment is finished, the pipette is discarded.

Other issue arises such as temperature control. As I mentioned above, the kinetics of currents are temperature dependent. All the experiments were done at room temperature in Medellin. This temperature can vary depending on the specific climate of the day.

The patch pipette must be positioned precisely on a micrometer scale. For this purpose, hydraulic (water) manipulator was damaged.

Recordings on sodium channels were not fully completed because of the time.

Other limitations:

• Delay due to closure of the Biophysics and PHYSIS laboratory located at the Faculty of Medicine of the University of Antioquia from 03-15-2020 to 10-15-2020 and from 12-20-2020 to 02-25-2021 (National quarantine for Covid-19). This laboratory is equipped with the essential equipment for the project execution.

• No availability of animals (mice) used for experimentation, given the closure of the Serpentarium of the University of Antioquia because of the pandemic, with which there is an agreement.

• Delay in purchasing inputs used for experiments.

• Mobility restrictions (quarantine / curfew) from Thursday to Monday implemented by the Government of Antioquia to the Medellin city. This measure affected admission to the Faculty of Medicine, since academic activities could only be carried out from Wednesday to Saturday.

• Diagnosis of Covid19 twice.

• Two domestic calamities.

Funding: Producing this body of research would not have been possible without the funding received from the University of Antioquia three-Year Fellowship (*Estudiante Instructor*).

I gratefully acknowledge the funding received towards my Master from the project *Síntesis y caracterización de péptidos a partir de venenos de arañas: hacia el desarrollo de nuevos antimicrobianos*, code 111577757673, financed by the Ministry of Science, Technology and Innovation, Colombia.

I am also grateful to the funding received through the Biophysics (https://bit.ly/3n4dNW6, https://n9.cl/9pnlu) and PHYSIS (www.udea.edu.co/physis, https://n9.cl/ory88) groups for providing the facilities, materials and equipment I needed to undertake my Master.

Conflict of interests: The authors declare no conflicts of interest associated with this study.

Chapter 12
References

Ackers-Johnson, M., Li, P. Y., Holmes, A. P., O'Brien, S. M., Pavlovic, D. en Foo, R. S. (2016). A Simplified, Langendorff-Free Method for Concomitant Isolation of Viable Cardiac Myocytes and Nonmyocytes from the Adult Mouse Heart. *Circ. Res.* **119**, 909–920.

Adams, J. (2004). The development of proteasome inhibitors as anticancer drugs. *Cancer Cell* 5(5), 417–421.

Agwa, A. J., Tran, P., Mueller, A., Tran, H. N. T., Deuis, J. R., Israel, M. R., McMahon, K. L., Craik, D. J., Vetter, I. en Schroeder, C. I. (2020). Manipulation of a spider peptide toxin alters its affinity for lipid bilayers and potency and selectivity for voltage-gated sodium channel subtype 1.7. *J. Biol. Chem.*

Attali, B., Chandy, K. G., Giese, M. H., Grissmer, S., Gutman, G. A., Jan, L. Y., Lazdunski, M., Mckinnon, D., Nerbonne, J., Pardo, L. A., Robertson, G. A., Rudy, B., Sanguinetti, M. C., Stühmer, W., Trimmer, J. S. and Wang, X. (2019). Voltage-gated potassium channels (version 2019.4). *UPHAR/BPS Guid. to Pharmacol. Database*.

Bahar, A. A. en Ren, D. (2013). Antimicrobial peptides. *Pharmaceuticals* **6**, 1543–1575.

Balse, E., Steele, D. F., Abriel, H., Coulombe, A., Fedida, D. en Hatem, S. N. (2012). Dynamic of ion channel expression at the plasma membrane of cardiomyocytes. *Physiol. Rev.* **92**, 1317–1358.

Bell, R. M., Mocanu, M. M. en Yellon, D. M. (2011). Retrograde heart perfusion: The Langendorff technique of isolated heart perfusion. *J. Mol. Cell. Cardiol.* **50**, 940–950.

Bernèche, S. en Roux, B. (2001). Energetics of ion conduction through the K+ channel. *Nature* **414**, 73–77.

Blanc, E., Romi-Lebrun, R., Bornet, O., Nakajima, T. en Darbon, H. (1998). Solution structure of two new toxins from the venom of the Chinese scorpion Buthus martensi karsch blockers of potassium channels. *Biochemistry* **37**, 12412–12418.

Bordon, K. de C. F., Cologna, C. T., Fornari-Baldo, E. C., Pinheiro-Júnior, E. L., Cerni, F. A., Amorim, F. G., Anjolette, F. A. P., Cordeiro, F. A., Wiezel, G. A., Cardoso, I. A., et al. (2020). From Animal Poisons and Venoms to Medicines: Achievements, Challenges and Perspectives in Drug Discovery. *Front. Pharmacol.* **11**,.

Boron, W. en Boulpaep, E. (2012). *Medical Physiology*. Second edi.

Burrows, M. T. (1910). The cultivation of tissues of the chick-embryo outside the body. *J. Am. Med. Assoc.* **55**, 2057–2058.

Campora, S., Alberte, P. S., Bruno, C. en Ghersi, G. (2018). Isolation of adult rat cardiomyocytes using recombinant collagenases. *Chem. Eng. Trans.* **64**, 25–30.

Catterall, W. A. (1995). Structure and function of voltage-gated ion channels. *Annu. Rev. Biochem.* 64(1), 493–531.

Catterall, W. A., Cestèle, S., Yarov-Yarovoy, V., Yu, F. H., Konoki, K. en Scheuer, T. (2007). Voltage-gated ion channels and gating modifier toxins. *Toxicon* 49(2), 124–141.

Catterall, W. A., Perez-Reyes, E., Snutch, T. P. en Striessnig, J. (2021). Voltage-gated calcium channels (Ca_V) in GtoPdb v.2021.3. *IUPHAR/BPS Guid. to Pharmacol. CITE* **2021**,.

Cecchi, X., Wolff, D., Alvarez, O. en Latorre, R. (1987). Mechanisms of Cs+ blockade in a Ca2+-activated K+ channel from smooth muscle. *Biophys. J.* **52**, 707–716.

Chen, C. C., Cang, C., Fenske, S., Butz, E., Chao, Y. K., Biel, M., Ren, D., Wahl-Schott, C. en Grimm, C. (2017). Patch-clamp technique to characterize ion channels in enlarged individual endolysosomes. *Nat. Protoc.* **12**, 1639–1658.

Choe, S. (2002). Ion channel structure: Potassium channel structures. *Nat. Rev. Neurosci.* 3(2), 115-121.

Chong, Y., Hayes, J. L., Sollod, B., Wen, S., Wilson, D. T., Hains, P. G., Hodgson, W. C., Broady, K. W., King, G. F. en Nicholson, G. M. (2007). The ω-atracotoxins: Selective blockers of insect M-LVA and HVA calcium channels. *Biochem. Pharmacol.* **74**, 623–638.

Cifuentes, Y., Estrada-Gomez, S., Vargas-Muñoz, L. J. en Perafán, C. (2016). Description and molecular characterization of a new species of tarantula, pamphobeteus verdolaga, from colombia (Araneae: Mygalomorphae: Theraphosidae). *Zoologia* 33.

Coetzee, W. A., Amarillo, Y., Chiu, J., Chow, A., Lau, D., McCormack, T., Moreno, H., Nadal, M. S., Ozaita, A., Pountney, D., et al. (1999). Molecular diversity of K+ channels. In *Annals of the New York Academy of Sciences*, bll 868(1), 233–255.

Daroff, R. B., & Aminoff, M. J. (2014). *Encyclopedia of the neurological sciences. Academic press.*

Dathe, M. en Wieprecht, T. (1999). Structural features of helical antimicrobial peptides: Their potential to modulate activity on model membranes and biological cells. *Biochim. Biophys. Acta - Biomembr.* **1462**, 71–87.

Deuis, J. R., Dekan, Z., Wingerd, J. S., Smith, J. J., Munasinghe, N. R., Bhola, R. F., Imlach, W. L., Herzig, V., Armstrong, D. A., Rosengren, K. J., et al. (2017). Pharmacological characterisation of the highly Na v 1.7 selective spider venom peptide Pn3a. *Sci. Rep.* **7**, 1–18.

Doyle, D. A., Cabral, J. M., Pfuetzner, R. A., Kuo, A., Gulbis, J. M., Cohen, S. L., Chait, B. T. en MacKinnon, R. (1998). The structure of the potassium channel: Molecular basis of K+ conduction and selectivity. *Science (80-.).* **280**, 69–77.

Escoubas, P., Diochot, S. en Corzo, G. (2000). Structure and pharmacology of spider venoms neurotoxins. *Biochimie* **82**, 893–907.

Estrada-Gomez, S., Vargas Muñoz, L. J. en Quintana Castillo, J. C. (2013). Extraction and partial characterization of venom from the Colombian spider Pamphobeteus aff. nigricolor (Aranae:Theraphosidae). *Toxicon* 76, 301–309.

Farre, C. en Fertig, N. (2012). HTS techniques for patch clamp-based ion channel screening - Advances and economy. *Expert Opin. Drug Discov.* 7(6), 515–524.

Farre, C., Stoelzle, S., Haarmann, C., George, M., Brüggemann, A. en Fertig, N. (2007). Automated ion channel screening: Patch clamping made easy. *Expert Opin. Ther. Targets* 11(4), 557–565.

Ferdinandy, P., Schulz, R. en Baxter, G. F. (2007). Interaction of cardiovascular risk factors with myocardial ischemia/reperfusion injury, preconditioning, and postconditioning. *Pharmacol. Rev.* **59**, 418–458.

Fertig, N., Blick, R. H. en Behrends, J. C. (2002). Whole cell patch clamp recording performed on a planar glass chip. *Biophys. J.* 82(6), 3056–3062.

Fraser, S. P., Ozerlat-Gunduz, I., Brackenbury, W. J., Fitzgerald, E. M., Campbell, T. M., Coombes, R. C. en Djamgoz, M. B. A. (2014). Regulation of voltage-gated sodium channel expression in cancer: Hormones, growth factors and auto-regulation. *Philos. Trans. R. Soc. B Biol. Sci.* 369(1638), 20130105.

Frazão, B., Vasconcelos, V. en Antunes, A. (2012). Sea anemone (cnidaria, anthozoa, actiniaria) toxins: An overview. *Mar. Drugs* 10(8), 1812–1851.

Goldin, A. L., Barchi, R. L., Caldwell, J. H., Hofmann, F., Howe, J. R., Hunter, J. C., Kallen, R. G., Mandel, G., Meisler, M. H., Netter, Y. B., et al. (2000). Nomenclature of voltage-gated sodium channels. *Neuron* 28(2), 365–368.

Grant, A. O. (2009). Cardiac ion channels. *Circ. Arrhythmia Electrophysiol.* **2**, 185–194.

Greg Ikonnikov and Dominique Yelle (2018). Physiology of cardiac conduction and contractility. Review, 40(11), 1053-64.

Gutman, G. A., Chandy, K. G., Adelman, J. P., Aiyar, J., Bayliss, D. A., Clapham, D. E., Covarriubias, M., Desir, G. V., Furuichi, K., Ganetzky, B., et al. (2003). International Union of Pharmacology. XLI. Compendium of Voltage-Gated Ion Channels: Potassium Channels. *Pharmacol. Rev.* 55(4), 583–586.

Heginbotham, L. en MacKinnon, R. (1992). The aromatic binding site for tetraethylammonium ion on potassium channels. *Neuron* **8**, 483–491.

Heginbotham, L., Lu, Z., Abramson, T. en MacKinnon, R. (1994). Mutations in the K+ channel signature sequence. *Biophys. J.* **66**, 1061–1067.

Henriques, S. T., Deplazes, E., Lawrence, N., Cheneval, O., Chaousis, S., Inserra, M., Thongyoo, P., King, G. F., Mark, A. E., Vetter, I., et al. (2016). Interaction of tarantula venom peptide ProTx-II with lipid membranes is a prerequisite for its inhibition of human voltage-gated sodium channel NaV 1.7. *J. Biol. Chem.* **291**, 17049–17065.

Herzig, V., Wood, D. L. A., Newell, F., Chaumeil, P. A., Kaas, Q., Binford, G. J., Nicholson, G. M., Gorse, D. en King, G. F. (2011). ArachnoServer 2.0, an updated online resource for spider toxin sequences and structures. *Nucleic Acids Res.* 39(suppl_1), D653–D657.

Hodgkin, A. L. en Huxley, A. F. (1952a). The dual effect of membrane potential on sodium conductance in the giant axon of Loligo. *J. Physiol.* **116**, 497–506.

Hodgkin, A. L. en Huxley, A. F. (1952b). A quantitative description of membrane current and its application to conduction and excitation in nerve. *J. Physiol.* **117**, 500–544.

Hodgkin, A. en Huxley, A. (1952c). A quantitative description of membrane current and its application to conductance and excitation. *J. Physiol.* **117**, 500–44.

Hodgkin, A. L. en Huxley, A. F. (1952d). Currents carried by sodium and potassium ions through the membrane of the giant axon of Loligo. *J. Physiol.* **116**, 449–472.

Hodgkin, A. L., Huxley, A. F. en Katz, B. (1952). Measurement of current-voltage relations in the membrane of the giant axon of Loligo. *J. Physiol.* **116**, 424–448.

HODGKIN, A. L. en HUXLEY, A. F. (1952). Propagation of electrical signals along giant nerve fibers. *Proc. R. Soc. Lond. B. Biol. Sci.* **140**, 177–183.

Hu, Z., Zhou, X., Chen, J., Tang, C., Xiao, Z., Ying, D., Liu, Z. en Liang, S. (2014). The venom of the spider Selenocosmia jiafu contains various neurotoxins acting on voltage-gated ion channels in rat dorsal root ganglion neurons. *Toxins (Basel).* **6**, 988–1001.

Huang, P. T., Shiau, Y. S. en Lou, K. L. (2007). The interaction of spider gating modifier peptides with voltage-gated potassium channels. *Toxicon* 49(2), 285–292.

Huang, H., Pugsley, M. K., Fermini, B., Curtis, M. J., Koerner, J., Accardi, M. en Authier, S. (2017). Cardiac voltage-gated ion channels in safety pharmacology: Review of the

landscape leading to the CiPA initiative. *J. Pharmacol. Toxicol. Methods* **87**, 11–23.

Hucho, F. en Weise, C. (2001). Ligand-gated ion channels. *Angew. Chemie - Int. Ed.* **40**, 3100–3116.

Huxley, A. F. (1952a). J. Physiol. (I952). 449–472.

Huxley, F. (1952b). Laboratory of. 497–506.

Huxley, A. F. en Hodgkin, B. Y. A. L. (1952). The components of membrane conductance in the giant axon of Loligo. *J. Physiol.* 473–496.

IUPHAR/BPS Guide to PHARMACOLOGY (2022). Cs+.

James L. Rae; Richard A. Levis (1992). of Physiology Short communication A method for exceptionally low noise single channel recordings. 618–620.

Jiang, D., Shi, H., Tonggu, L., Gamal El-Din, T. M., Lenaeus, M. J., Zhao, Y., Yoshioka, C., Zheng, N. en Catterall, W. A. (2020). Structure of the Cardiac Sodium Channel. *Cell* **180**, 122-134.e10.

Johnston en Wu (1995). *Foundations of cellular neurophysiology*.

King, G. F., Escoubas, P. en Nicholson, G. M. (2008a). Peptide toxins that selectively target insect NaV and Ca V channels. *Channels* 2(2), 100–116.

King, G. F., Escoubas, P. en Nicholson, G. M. (2008b). Peptide toxins that selectively target insect NaV and Ca V channels. *Channels* **2**, 100–116.

King, G. F., Gentz, M. C., Escoubas, P. en Nicholson, G. M. (2008c). A rational nomenclature for naming peptide toxins from spiders and other venomous animals. *Toxicon* **52**, 264–276.

Klint, J. K., Senff, S., Rupasinghe, D. B., Er, S. Y., Herzig, V., Nicholson, G. M. en King, G. F. (2012). Spider-venom peptides that target voltage-gated sodium channels: Pharmacological tools and potential therapeutic leads. *Toxicon* 60(4), 478–491.

Kolb, I., Stoy, W. A., Rousseau, E. B., Moody, O. A., Jenkins, A. en Forest, C. R. (2016). Cleaning patch-clamp pipettes for immediate reuse. *Sci. Rep.* **6**, 1–10.

Levis, R. A. en Rae, J. L. (1998). Low-noise patch-clamp techniques. *Methods Enzymol.* **293**, 218–266.

Lewis, R. J., Dutertre, S., Vetter, I. en Christie, M. J. (2012). Conus venom peptide pharmacology. *Pharmacol. Rev.* 64(2), 259–298.

Li, D., Wu, J., Bai, Y., Zhao, X. en Liu, L. (2014). Isolation and culture of adult mouse cardiomyocytes for cell signaling and in vitro cardiac hypertrophy. *J. Vis. Exp.* (87).

Li, H., Liu, C., Bao, M., Liu, W., Nie, Y., Lian, H. en Hu, S. (2020). Optimized Langendorff perfusion system for cardiomyocyte isolation in adult mouse heart. *J. Cell. Mol. Med.* **24**, 14619–14625.

Lingwood, D. en Simons, K. (2010). Lipid rafts as a membrane-organizing principle. *Science (80-.).* **327**, 46–50.

Liu, B., Li, A., Qin, Y., Tian, X., Gao, M., Jiang, W. en Gong, G. (2019). Comparative study on isolation and mitochondrial function of adult mouse and rat cardiomyocytes. *J. Mol. Cell. Cardiol.* **136**, 64–71.

Lu, Q. en An, W. (2008). Impact of Novel Screening Technologies on Ion Channel Drug Discovery. *Comb. Chem. High Throughput Screen.* **11**, 185–194.

Maier, S. K. G., Westenbroek, R. E., Schenkman, K. A., Feigl, E. O., Scheuer, T. en Catterall, W. A. (2002). An unexpected role for brain-type sodium channels in coupling of

cell surface depolarization to contraction in the heart. *Proc. Natl. Acad. Sci. U. S. A.* **99**, 4073–4078.

Maltsev, V. A., Wobus, A. M., Rohwedel, J., Bader, M. en Hescheler, J. (1994). Cardiomyocytes differentiated in vitro from embryonic stem cells developmentally express cardiac-specific genes and ionic currents. *Circ. Res.* **75**, 233–244.

Männikkö, R., Shenkarev, Z. O., Thor, M. G., Berkut, A. A., Myshkin, M. Y., Paramonov, A. S., Kulbatskii, D. S., Kuzmin, D. A., Castañeda, M. S., King, L., et al. (2018). Spider toxin inhibits gating pore currents underlying periodic paralysis. *Proc. Natl. Acad. Sci. U. S. A.* 115(17), 4495–4500.

Manual, I. PUL-1000.

McDonough, S. I. (2007). Gating modifier toxins of voltage-gated calcium channels. *Toxicon* **49**, 202–212.

McGivern, J. G. (2007). Advantages of voltage-gated ion channels as drug targets. *Expert Opin. Ther. Targets* **11**, 265–271.

Mesirca, P., Torrente, A. G. en Mangoni, M. E. (2015). Functional role of voltage gated Ca2+ channels in heart automaticity. *Front. Physiol.* **6**, 19.

Mitcheson, J. S., Hancox, J. C. en Levi, A. J. (1998). Cultured adult cardiac myocytes: Future applications, culture methods, morphological and electrophysiological properties. *Cardiovasc. Res.* **39**, 280–300.

Moore, J. W. en Cole, K. S. (1963). Voltage clamp techniques. In *Electrophysiological Methods*, bl (pp. 263-321).

Mortensen, M. en Smart, T. G. (2007). Single-channel recording of ligand-gated ion channels. *Nat. Protoc.* **2**, 2826–2841.

Neher, E. en Sakmann, B. (1976). Single-channel currents recorded from membrane of denervated frog muscle fibres. *Nature* 260(5554), 799–802.

Nguyen, L. T., Haney, E. F. en Vogel, H. J. (2011). The expanding scope of antimicrobial peptide structures and their modes of action. *Trends Biotechnol.* **29**, 464–472.

Niwa, N., Yasui, K., Opthof, T., Takemura, H., Shimizu, A., Horiba, M., Lee, J. K., Honjo, H., Kamiya, K. en Kodama, I. (2004). Cav3.2 subunit underlies the functional T-type Ca2+ channel in murine hearts during the embryonic period. *Am. J. Physiol. - Hear. Circ. Physiol.* **286**,.

Noda, M., Ikeda, T., Suzuki, H., Takeshima, H., Takahashi, T., Kuno, M. en Numa, S. (1986). Expression of functional sodium channels from cloned cDNA. *Nature* 322(6082), 826–828.

Nuss, H. B. en Marban, E. (1994). Electrophysiological properties of neonatal mouse cardiac myocytes in primary culture. *J. Physiol.* **479**, 265–279.

Olivera, B. M. (1997). E.E. Just lecture, 1996. Conus venom peptides, receptor and ion channel targets, and drug design: 50 million years of neuropharmacology. In *Molecular Biology of the Cell*, bll 8, 2101–2109.

Onkal, R. en Djamgoz, M. B. A. (2009). Molecular pharmacology of voltage-gated sodium channel expression in metastatic disease: Clinical potential of neonatal Nav1.5 in breast cancer. *Eur. J. Pharmacol.* **625**, 206–219.

Pascual, J. M., Shieh, C. C., Kirsch, G. E. en Brown, A. M. (1995). Multiple residues specify external tetraethylammonium blockade in voltage-gated potassium channels. *Biophys. J.* **69**, 428–434.

Platzer, D. en Zorn-Pauly, K. (2020). Accuracy considerations for capacitance estimation by

voltage steps in cardiomyocytes. *Prog. Biophys. Mol. Biol.* **157**, 3–10.

Possani, L. D., Merino, E., Corona, M., Bolivar, F. en Becerril, B. (2000). Peptides and genes coding for scorpion toxins that affect ion-channels. *Biochimie* 82(9–10), 861–868.

Pringos, E., Vignes, M., Martinez, J. en Rolland, V. (2011). Peptide neurotoxins that affect voltage-gated calcium channels: A close-up on ω-agatoxins. *Toxins (Basel).* **3**, 17–42.

Ranjan, R., Logette, E., Marani, M., Herzog, M., Tâche, V., Scantamburlo, E., Buchillier, V. en Markram, H. (2019). A Kinetic Map of the Homomeric Voltage-Gated Potassium Channel (Kv) Family. *Front. Cell. Neurosci.* **13**,.

Rash, L. D. en Hodgson, W. C. (2002). Pharmacology and biochemistry of spider venoms. *Toxicon* **40**, 225–254.

Reuter, H. (2013). *Voltage-Gated Ca2+ Channels*. 2nd ed Elsevier Inc.

Robertson, C., Tran, D. D. en George, S. C. (2013). Concise review: Maturation phases of human pluripotent stem cell-derived cardiomyocytes. *Stem Cells* **31**, 829–837.

Rolf, S., Haverkamp, W., Borggrefe, M., Mußhoff, U., Eckardt, L., Mergenthaler, J., Snyders, D. J., Pongs, O., Speckmann, E. J., Breithardt, G., et al. (2000). Effects of antiarrhythmic drugs on cloned cardiac voltage-gated potassium channels expressed in Xenopus oocytes. *Naunyn. Schmiedebergs. Arch. Pharmacol.* **362**, 22–31.

Rougier, J. S. en Abriel, H. (2016). Cardiac voltage-gated calcium channel macromolecular complexes. *Biochim. Biophys. Acta - Mol. Cell Res.* **1863**, 1806–1812.

Sack, J. T. (2017). The envenomation of general physiology throughout the last century. *J. Gen. Physiol.* **149**, 975–983.

Sakmann, B., Hamill, O. P., Sigworth, F. J., Marty, A. en Neher, E. (1981). Improved patch-clamp techniques for high-resolution current recording from cells and cell-free membrane patches. *Pflügers Arch. - Eur. J. Physiol.* **391**, 85–100.

Senatore, A., Raiss, H. en Le, P. (2016). Physiology and evolution of voltage-gated calcium channels in early diverging animal phyla: Cnidaria, placozoa, porifera and ctenophora. *Front. Physiol.* **7**, 1–26.

Sigworth, F. J. (1983). Electronic Design of the Patch Clamp. *Single-Channel Rec.* 3–35.

Singer, S. . en Nicolson, G. L. (1972). Singer1972.Pdf. *Science (80-.).* **175**, 720–731.

Single Barrel Capillary Glass Without Microfilament for Patch Clamp.

Smyth, M. S. en Martin, J. H. J. (2000). x Ray crystallography. *J. Clin. Pathol. - Mol. Pathol.* **53**, 8–14.

Snyders, D. J. (1999). Structure and function of cardiac potassium channels. *Cardiovasc. Res.* **42**, 377–390.

Synthase, A. A. O. A. T. P. (2013). *Encyclopedia of Biophysics*.

Takamori, S., Holt, M., Stenius, K., Lemke, E. A., Grønborg, M., Riedel, D., Urlaub, H., Schenck, S., Brügger, B., Ringler, P., et al. (2006). Molecular Anatomy of a Trafficking Organelle. *Cell* **127**, 831–846.

Tasaki, I. en Singer, I. (1968). SOME PROBLEMS INVOLVED IN ELECTRIC MEASUREMENTS OF BIOLOGICAL SYSTEMS. *Ann. N. Y. Acad. Sci.* **148**, 36–53.

Tester, M. (1997). Techniques for studying ion channels: An introduction. *J. Exp. Bot.* **48**, 353–359.

The Nobel Prize in Physiology or Medicine 1963.

The Nobel Prize in Physiology or Medicine 1991.

Vieira, L. B., Kushmerick, C., Hildebrand, M. E., Garcia, E., Stea, A., Cordeiro, M. N., Richardson, M., Gomez, M. V. en Snutch, T. P. (2005). Inhibition of high voltage-activated calcium channels by spider toxin PnTx3-6. *J. Pharmacol. Exp. Ther.* **314**, 1370–1377.

William, C. (2009). Structure and function of ion channels. *Eur. Biophys. J.* **38**, 271–272.

Williams, M., Raddatz, R., Mehlin, C. en Triggle, D. J. (2006). Receptor Targets in Drug Discovery. In *Encyclopedia of Molecular Cell Biology and Molecular Medicine*, bl Weinheim, Germany: Wiley-VCH Verlag GmbH & Co. KGaA.

Willumsen, N. J., Bech, M., Olesen, S. P., Jensen, B. S., Korsgaard, M. P. G. en Christophersen, P. (2003). High throughput electrophysiology: New perspectives for ion channel drug discovery. *Recept. Channels* 9(1), 3–12.

Wulff, H., Castle, N. A. en Pardo, L. A. (2009). Voltage-gated potassium channels as therapeutic targets. *Nat. Rev. Drug Discov.*

Xie, C., Lin, Z., Hanson, L., Cui, Y. en Cui, B. (2012). Intracellular recording of action potentials by nanopillar electroporation. *Nat. Nanotechnol.* **7**, 185–190.

Xiong, Z., Sperelakis, N. en Fenoglio-Preiser, C. (1994). Isoproterenol modulates the calcium channels through two different mechanisms in smooth-muscle cells from rabbit portal vein. *Pflügers Arch. Eur. J. Physiol.* **428**, 105–113.

Yamakage, M. en Namiki, A. (2002). Calcium channels - Basic aspects of their structure, function and gene encoding; anesthetic action on the channels - A review. *Can. J. Anesth.* **49**, 151–164.

Yan, S., Huang, P., Wang, Y., Zeng, X. en Zhang, Y. (2018). The venom of ornithoctonus huwena affect the electrophysiological stability of neonatal rat ventricular myocytes by inhibiting sodium, potassium and calcium current. *Channels* **12**, 109–118.

Yu, F. H., Yarov-Yarovoy, V., Gutman, G. A. en Catterall, W. A. (2005). Overview of molecular relationships in the voltage-gated ion channel superfamily. *Pharmacol. Rev.* 57(4), 387–395.

Zhang, Y. Y., Huang, Y., He, Q. Z., Luo, J., Zhu, L., Lu, S. S., Liu, J. Y., Huang, P. F., Zeng, X. Z. en Liang, S. P. (2015). Structural and functional diversity of peptide toxins from tarantula Haplopelma hainanum (Ornithoctonus hainana) venom revealed by transcriptomic, peptidomic, and patch clamp approaches. *J. Biol. Chem.* 290(22), 14192–14207.

Zhang, S. K., Song, J. W., Gong, F., Li, S. B., Chang, H. Y., Xie, H. M., Gao, H. W., Tan, Y. X. en Ji, S. P. (2016). Design of an α-helical antimicrobial peptide with improved cell-selective and potent anti-biofilm activity. *Sci. Rep.* **6**, 1–13.

Zhang, Y., Peng, D., Huang, B., Yang, Q., Zhang, Q., Chen, M., Rong, M. en Liu, Z. (2018). Discovery of a Novel Nav1.7 Inhibitor From Cyriopagopus albostriatus Venom With Potent Analgesic Efficacy. *Front. Pharmacol.* 9, 1158.

Zhao, Z., Lan, H., El-Battrawy, I., Li, X., Buljubasic, F., Sattler, K., Yücel, G., Lang, S., Tiburcy, M., Zimmermann, W. H., et al. (2018). Ion Channel Expression and Characterization in Human Induced Pluripotent Stem Cell-Derived Cardiomyocytes. *Stem Cells Int.* **2018**,.